Title
A CRITICAL REVIEW OF THE PEIERLS MECHANISM

Authors
Guyot, Pierre
Dorn, John E.

Publication Date
1966-07-01

UCRL-16992

University of California

Ernest O. Lawrence Radiation Laboratory

A CRITICAL REVIEW OF THE PEIERLS MECHANISM

DISCLAIMER

DISCLAIMER

Deformation of Crystalline Solids
Ottawa Conference, Aug. 1966

UCRL-16992

UNIVERSITY OF CALIFORNIA

Lawrence Radiation Laboratory
Berkeley, California

AEC Contract No. W-7406-eng-48

A CRITICAL REVIEW OF THE PEIERLS MECHANISM

Pierre Guyot and John E. Dorn

July, 1966

A CRITICAL REVIEW OF TEH PEIERLS MECHANISM

Pierre Guyot and John E. Dorn

Inorganic Materials Research Division, Lawrence Radiation Laboratory, and Department of Mineral Technology, College of Engineering, University of California, Berkeley, California

July, 1966

ABSTRACT

A thorough review is made of the application of the Peierls model to the macroscopic plastic deformation of ionic crystals, metals, alloys and covalently bonded crystals. The effects of the shape of the Peierls hill, kink-kink energies and the frequency terms on the stress-temperature and activation volume-stress relationships are extended and discussed. Theory is compared with experimental results giving special emphasis to recent advances. Single crystal data for 1/2[111]{110} thermally activated slip in Ta and Mo at low temperatures agree well with the dictates of the Peierls mechanism. Deformation characteristics of polycrystalline Fe alloys containing either 2 wt.% Mn or 11 at.% Mo agree with expectations based on the Peierls mechanism only at temperatures below about 200°K. At higher temperatures the effective stress decreases more slowly and the activation volume increases more rapidly with increasing temperature than can be accounted for by the Peierls mechanism. Over this higher temperature range, however, the experimental data are in good agreement with Escaig's mechanism based on the recombination of dissociated screw dislocations. It is also shown that low temperature 1/2[111]{123} slip in AgMg, prismatic slip in Ag plus 33 at.% Al, and in Mg plus 6 - 12 at.% Li occurs by the Peierls mechanism.

I. INTRODUCTION

As first noted by Peierls (1940), a straight dislocation has its minimum energy when it lies in a "valley" parallel to close-packed rows of atoms on its glide plane. When the dislocation is displaced from the bottom of the "valley" the configuration of atoms in its core is altered and its energy increases. Consequently the energy of a straight dislocation is a function of its displacement; the energy has the periodicity, a, of the spacing between the parallel rows of atoms. Therefore it is necessary to apply a certain force $\tau_p b$ per unit dislocation length, where b is the Burger's vector and τ_p is known as the Peierls stress, to move the dislocations over the Peierls hills mechanically. Estimates of this stress can be made in terms of variations in bond energies of atoms in the dislocation core as it is displaced. High Peierls stresses are expected in two cases, in covalently bonded crystalline materials where the bond energies are directionally sensitive, and in ionic crystals where the dislocation must overcome Coulombic interactions during glide. In contrast crystalline materials exhibiting exclusively metallic bonding are expected to have very small Peierls stresses. In f.c.c. metals, for example, the Peierls stress is so low that their low-temperature thermally-activated deformation is determined by the now more difficult intersection mechanism.

The first analyses for estimating the Peierls stress, such as those based on the Frenkel-Kontorova (1938), Peierls (1940), Nabarro (1952) and related models, served to identify some of the factors that are involved. The inherent crudity of these models and their notorious

sensitivity to the details of the assumptions that were made, however, detract from their utility. They invariably suggested unacceptably high estimates for the Peierls stress in metals. Recent analyses, based on Morse or Born-Mayer types of interactions potentials appear to give more acceptable values of the Peierls stress. The more physically realistic but exceedingly difficult quantum-mechanical approach for estimating the Peierls stress has only recently been probed, Susuki (1963); nevertheless his calculation is questionable, because he used the Friedel-Leman concept of tight bonding which is only valid in a perfect crystal.

In crystals where the Peierls stress is high, dislocations frequently assume polygonal shapes analogous to those, for example, that have been observed in Si, Lang (1958). The straight sections of such dislocations lie parallel to the more closely packed rows of atoms on the slip plane. For cases where the Peierls stress is low, however, as in f.c.c. metals, dislocations assume less regular shapes and, in general, cross over the low Peierls hills with only minor deviations. The decrease in energy, if the segments of such kinked dislocations were to be parallel to a series of Peierls valleys, is insufficient to provide for the greater dislocation line energy that would be required. Highly kinked dislocations move with great ease, by displacement of the kinks, even at extremely low temperatures, Seitz (1952), Brailsford (1961). It is not always necessary that the Peierls stress be high when dislocations lie parallel to close-packed rows of atoms. For example the dissociated screw and Cottrell-Lomer dislocations also take these orientations.

We will be interested here in crystals that have sufficiently high Peierls stresses to cause the dislocations to lie predominantly in the

Peierls valleys. The vibration of such dislocations under small oscillating stresses can induce thermally-activated nucleation of pairs of kinks that can account, at least partially, for the internal friction peaks often observed at low temperatures, Bordoni (1949), Seeger (1956). It will not, however, be our objective to describe these phenomena here. Rather we will emphasize only the macroscopic deformation of crystals when such deformation is dictated by the Peierls mechanism.

A critical comparison will be made of the several dislocation models that have been suggested for the nucleation of pairs of kinks. Then formulations of the macroscopic strain rate in terms of the stress, temperature and dislocation substructure will be reviewed and criticized. Finally the theoretical predictions will be compared with experimental data. The results for ionic and covalent crystals will be reviewed but special attention will be given to recent data on b.c.c. metals, several different alloys and intermetallic compounds.

Other mechanisms of deformation are competitive with the Peierls mechanism. The unique differences between the Peierls mechanism and that controlled by the intersection of dislocations provide a rather clear distinction between the two. The recently proposed mechanism of Escaig (1966) based on the recombination of dissociated screw dislocations in b.c.c. metals, although it is distinctly different in concept, nevertheless gives trends that are often somewhat similar to those suggested by the Peierls mechanism. We suggest that the recombination mechanism of Escaig might well account for the thermally activated deformation of Fe between about 170° and 400°K. On the other hand it appears to be

incompetent to account for the deformation of Fe below about 170°K where the results agree well with predictions made on the basis of the Peierls mechanism.

II. MODELS OF THE PEIERLS PROCESS

When the applied stress is zero, segments of dislocations tend to lie in the Peierls valleys parallel to close-packed rows of atoms on the slip plane. To move a dislocation out of its valley a shear stress τ^* equal to τ_p, the Peierls stress, must be applied to the slip plane in the direction of the Burger's vector. When a stress τ^* less than τ_p is applied, the dislocation will move, as shown in Fig. 1, from its original position $A_oB_oC_o$ in the valley to a parallel position ABC part way up the Peierls hill. No further motion will occur at the absolute zero. At higher temperatures, however, thermal fluctuations cause the dislocation to vibrate about its mean position. When, however, a local thermal fluctuation is sufficiently energetic, a critical size dislocation loop AB'C is produced which no longer returns to its original position. The two partial kinks AB' and B'C for all configurations exceeding the critical one move apart and the dislocation is advanced to the next equilibrium position A"B"C".

Although this constitutes the basic concept of the Peierls mechanism for thermally activated deformation, a number of simplified analytical approaches have been suggested by different authors. There exist three important points of departure among the various individual models. The first concerns the shape of the Peierls hill that have been studied,

namely, as illustrated in Fig. 2, (a) sinusoidal and its simple modifications that have a single peak and valley in the spacing period, Seeger (1956), Friedel (1964), Dorn and Rajnak (1964), (b_1 and b_2) parabolic, Celli et al. (1963) (c) broken bond (Celli et al. (1963), Suzuki (1963)) (d) quasi parabolic (vide Appendix I) and (e) camels-hump hill having two equal peaks and primary and secondary minima (vide Appendix II). Types "a" and "b" and "d" give purely empirical representations of possible Peierls' hills. The major virtue of the type "d" hill is that it permits a completely analytical solution of the Peierls process in closed form. In contrast the broken bond model of type "c" has semi-theoretical justification for covalent types of structures having rigid bonds where glide of dislocations is probably accomplished by successive breaking and remaking of bonds. The type "e" hill appears to have some theoretical justification. A specific case was deduced, Chang (1966), for edge dislocations lying in the (110) plane in Fe by relaxation techniques using a two atom interaction potential so adjusted as to give the known elastic behavior of Fe. Significantly, the camel's hump hill varies only modestly from the broken bond model of type "c".

The height and shape of the Peierls hill influences the equilibrium configuration of a single kink; higher Peierls hills e.g. cause the dislocation to cross more abruptly from one valley to the next thus affecting the kink energy. The height and shape of the Peierls hills also influence the critical configuration and therefore the energy for nucleating a pair of kinks. On the other hand, as will be demonstrated later, the ratio of the energy to nucleate a pair of kinks under an

applied stress τ^* to the energy of an isolated kink depends primarily on τ^*/τ_p and is somewhat insensitive to the height and shape of the Peierls hills. For this reason it appears rather unlikely that good estimates of the details of the Peierls hills, other than the Peierls stress itself, might be obtained from experimental data on the Peierls mechanism.

A second point of departure in the analyses of different authors concerns the basis and approximations made for estimating the critical configuration for nucleating a pair of kinks. Each of the various approaches appears to coincide with physical reality only over special limited regions of the applied stress τ^*. A critical discussion of these issues will be given in the following section.

A third departure concerns the assumptions and the details of estimating the macroscopic strain rate in terms of nucleation and migration of kink pairs. This concerns the various viewpoints that have or may be adopted to estimate the preexponential term that must be multiplied by the Boltzmann factor in determining the shear-strain rate. These issues will also be discussed in the following section.

III. FORMULATION OF THE PEIERLS MECHANISM

A. Energy to Nucleate a Pair of Kinks

All estimates of the energy that must be supplied by a local thermal fluctuation in order to nucleate a pair of kinks have, thus far, been based on the simple line energy model of a dislocation. $\Gamma(y)$ is taken to be the energy per unit length of a dislocation where y is defined as shown in Fig. 1. Therefore the line energy is a periodic function of y

with a period a. The known variations of line energy with curvature and proportions of edge and screw orientations are neglected. Under a stress τ^* the stable equilibrium position of an infinitely long dislocation is $y = yo$. For any deviation from this position an energy

$$U = \int_{-\infty}^{\infty} \{\Gamma(y) \left[1 + \left(\frac{dy}{dx}\right)^2\right]^{1/2} - \Gamma(yo) - \tau^* b\,(y-yo)\}\, dx \qquad (1)$$

must be supplied externally. The equilibrium conditions obtained by taking extremal values of U are given by Euler's condition that

$$\tau^* b = \frac{d}{dy}\left\{\Gamma(y) \Big/ \sqrt{1 + \left(\frac{dy}{dx}\right)^2}\right\} \qquad (2)$$

U has its minimum value of zero for the condition of stable equilibrium when $y = yo$. An infinite number of alternate solutions are also obtainable but we limit our interest to that case which refers to a single pair of kinks centered about $x = 0$. For this case the boundary conditions for the integration of the equilibrium condition, Eq. (2), are

$$y = yo \text{ and } dy/dx = 0 \qquad \text{at } x = \pm\infty$$

$$y = yc \text{ and } dy/dx = 0 \qquad \text{at } x = 0$$

where yc is given by

$$\Gamma(yc) = \tau^* b\,(yc-yo) + \Gamma(yo)$$

The slope, dy/dx, of the critical pair of kinks is obtained by introducing the boundary conditions into the first integration of Eq. 2. As shown by Dorn and Rajnak (1964), when this slope is reintroduced into Eq. (1)

and the independent variable is changed from x to y

$$Un = 2 \int_{yo}^{yc} \{\Gamma(y)^2 - [\tau^* b(y-yo) + \Gamma(yo)]^2\}^{1/2} \, dy \qquad (3)$$

where Un now refers to the energy that must be supplied by a thermal fluctuation in order to nucleate a pair of kinks at the center of an infinitely long dislocation. This formulation neglects effects that arise in dislocation segments of finite length which may be restrained to remain at y = 0 at their terminal points on the slip plane. Arsenault (1966) has recently calculated Un for the formation of pairs of kinks in the center of dislocations of finite length. He finds, e.g. in the case of Fe, that Un reaches a constant value for dislocation segments longer than about 40b. This suggests that such end effects are of secondary importance in rather long dislocations.

To nucleate a pair of kinks when the applied stress is zero requires a thermal fluctuation having twice the energy of an isolated kink, i.e. $2U_k$. Applying the same analytical techniques as those described above gives

$$U_k = \Gamma o \int_{-a/2}^{a/2} \{\frac{\Gamma(y)}{\Gamma o} - 1\}^{1/2} \, dy \qquad (4)$$

The values of U_n and U_k can be determined by introducing appropriate values of $\Gamma(y)$ into Eqs. (3) and (4). We will consider only the following illustrative cases here:

$$\Gamma(y) = \frac{\Gamma c+\Gamma o}{2} + \frac{\Gamma c-\Gamma o}{2} \left(\frac{\alpha}{4} + \cos \frac{2\pi y}{a} - \frac{\alpha}{4} \cos \frac{4\pi y}{a}\right) \qquad (5a)$$

and

$$\Gamma(y) = \Gamma_o^{1/2} \left[\Gamma_o + \frac{ab\tau_p}{2}\left(1 - \frac{4y^2}{a^2}\right)\right]^{1/2} \qquad (5b)$$

Eq. (5a) gives a sinusoidal Peierls hill (Fig. 2a) when $\alpha = 0$, modified sinusoidal hills (Fig. 2a) when $-1 < \alpha < +1$, and the camel's hump hill, Fig. 2e, (which is also similar to the broken bond hill, Fig. 2c) when $\alpha > 1$. Eq. (5b) gives the quasi-parabolic hill, Fig. 2d. When a stress τ^* less than τ_p is applied to the slip plane of a lattice having a Peierls hill represented by Eq. (5a), dislocations are displaced to y_o where

$$\tau^* b = \frac{\alpha}{a}(\Gamma c - \Gamma o) \sin\frac{2\pi y_o}{a}\left(1 - \alpha\cos\frac{2\pi y_o}{a}\right) \qquad (6a)$$

The Peierls stress in this case is given by

$$\tau_p b = \frac{(\Gamma c - \Gamma o)}{16a|\alpha|}\left(3 + \sqrt{1 + 8\alpha^2}\right)\sqrt{8\alpha^2 - 2 + 2\sqrt{1 + 8\alpha^2}} \qquad (6b)$$

For these types of hills

$$\Gamma c = \Gamma m \qquad \text{over } -1 \leq \alpha \leq 1 \qquad (7a)$$

and

$$\Gamma c = \frac{2\Gamma m - \Gamma o\left(1 - \frac{1}{2\alpha} - \frac{\alpha}{2}\right)}{1 + \frac{1}{2\alpha} + \frac{\alpha}{2}} \qquad \text{over } 1 \leq \alpha \leq \infty \qquad (7b)$$

Consequently analyses are conveniently made using $R = \Gamma m/\Gamma o$ and α as the independent variables. On the other hand when the kink energy, U_k and the energy to nucleate a pair of kinks, U_n, are given in terms of the Peierls stress, τ_p, the line energy, Γo, and α, the results are insensitive

to variations in R over physically acceptable ranges.

When $\alpha = 0$, Eq. (4) can be integrated analytically (Seeger (1956) and Dorn and Rajnak (1964)) to give

$$U_k = \frac{2\Gamma_o a}{\pi}\left(\frac{2\tau_p ab}{\pi\Gamma_o}\right)^{1/2} \qquad (8a)$$

The corresponding relationship for the quasi-parabolic hill (vide Appendix I) is practically identical, namely

$$U_k = \pi^{3/2}\frac{\Gamma_o a}{8}\left(\frac{2\tau_p ab}{\pi\Gamma_o}\right)^{1/2} \qquad (8b)$$

illustrating that the results when expressed in terms of the Peierls stress and line energy are not only insensitive to R but also to variations in the shapes of the Peierls hills.

When $\alpha \neq 0$ analytical expressions for U_k can only be established by introducing simplifying assumptions such as for example $dy/dx << 1$ (Seeger (1956) and Celli et al. (1963)). This obviously eliminates considerations of abrupt kinks. However, rigorous numerical integration of Eq. (4) (Dorn and Mitchell (1964) and vide Appendix II) give the results shown in Fig. 3. The datum point at $\alpha = 0$ refers to results for the quasi-parabolic hill. Thus the kink energies depend primarily on Γ_o and τ_p and varies only modestly as the hill shape factor α increases.

For the quasi-parabolic hill, Eq. (5b), U_n can be obtained by direct analytical integration of Eq. (3) (vide Appendix I); and for the line energy of Eq. (5a), U_n has been obtained by numerical integration of Eq. (3) (Dorn and Rajnak (1964) and Appendix II). These type data, which are summarized in Fig. 4 for the quasi-parabolic hill and sinusoidal hills where $-1 \leq \alpha \leq 1$ and in Fig. A.2.1 for camel hump hills where

$\alpha > 1$ show that $U_n/2U_k$ is a simple function of τ^*/τ_p that is insensitive to R over the physically acceptable ranges. In general this function varies only modestly for several shapes of Peierls hills that were considered and becomes significantly different only for the camel hump hills.

Neither the Dorn-Rajnak (1964) nor the Friedel (1964) formulation of the energy to nucleate a pair of kinks considered directly the elastic kink-kink interaction energy. For abrupt kinks (Kroupa and Brown (1961) Wallace, Nunes and Dorn (1965)) of height $h = y_c - y_o$, this interaction energy is

$$U_{kk} = - \frac{\Gamma o}{4\pi} \frac{h^2}{w} \qquad (9)$$

where w is the kink separation. Since the dislocation line energy model always gives small values for h^2/w, U_{kk} is always small relative to U_n. This is illustrated in Appendix I where it is shown that for the quasi-parabolic model U_{kk}/U_n is a constant equal to 0.032.

In his approach to the problem Seeger (1956) assumed that the critical configuration consisted of two half-kinks separated by a distance w_c, as shown by curve (a) of Fig. 5, where w_c is determined as the width at which the applied stress overcomes the kink-kink attraction. On this basis Seeger suggests that

$$U_n = U_k + (\Gamma_c - \Gamma_o)\, w_c$$

and arrives at the relationship

$$U_n = U_k \left\{1 + 1/4 \ln \frac{16\tau_p}{\pi\tau^*}\right\} \qquad (10)$$

which he claims applies to sinusoidal hills at low values of the applied stress. As discussed previously, however, the kink-kink interaction energy is only a small fraction of the total line energy for the nucleation of a pair of kinks. It is not surprising therefore that Eq. (10) gives incorrect results, even when $\tau^* \to 0$ where U_n must obviously equal $2U_k$. While Seeger's assumption that the dislocation remains at the bottom of the Peierls hill at $y = -a/2$ is not serious for low stresses, it does not apply, excepting for the quasi-parabolic hill, for higher values of the applied stress. Furthermore, the dislocation line energy model suggests that y_c is not zero, as assumed by Seeger, but decreases from positive to negative values as the applied stress is increased. These factors suggest that several of the details incorporated in to the Seeger model are highly questionable.

Friedel (1964) was to first suggest that a line energy model rather than a kink-kink interaction model would prove to be more realistic. He assumed that the critical configuration might be deduced from the arrangement given by curve b of Fig. 5. This model, although based on line energy, yet retains some arbitrary features similar to those used by Seeger. As suggested by Friedel, his model may not be too seriously in error, however, at intermediate values of the applied stress.

The Lothe-Hirth (1959) theory assumes that number of kinks present is dictated by conditions of thermal equilibrium in the absence of a stress. They suggest that the rate with which kinks move depends on their stress directed diffusion. Obviously such a quasi-equilibrium theory can only apply when the stresses are extremely low.

It appears that the line energy formulations proposed by Celli et al. (1963) and Dorn and Rajnak (1964) provide the best currently available approaches for estimating the activation energy for nucleating pairs of kinks.

Several other mechanisms appear to give about the same trends of the effect of the applied stress on the activation energy as the Peierls mechanism based on nucleation of pairs of kinks. Some of these, however, can be distinguished from the Peierls mechanism in terms of the activation volume, which is given by

$$v^* = -\partial U_n / \partial \tau^* = -\frac{2U_k}{\tau_p} \frac{\partial\left(\frac{U_n}{2U_k}\right)}{\partial\left(\frac{\tau^*}{\tau_p}\right)} \qquad (11)$$

for the Peierls mechanism. For acceptable ranges of the kink energies and the Peierls stresses, such activation volumes usually range from 5 to 50 b^3, independent of dislocation density or the work hardened state. As shown in Fig. 6 the activation volumes are only modestly dissimilar for the various models of the Peierls hills and decrease as τ^*/τ_p increases. Here again only hills for which $\alpha > 1$ (vide Fig. A.2.2) give somewhat uniquely different trends. In general these results differ appreciably from those obtained when the intersection mechanism is valid where the activation volumes are about one order or more in magnitude larger and decrease with increased density of dislocations.

B. Kinetic Equations

A number of authors (Celli et al. (1964), Friedel (1964), Jøssang et al. (1963), Seeger et al. (1957)) have described the formulation of

the forward velocity of dislocations and the strain rate resulting from the nucleation of pairs of kinks. (Vide Brailsford (1961) regarding the redistribution of existing kinks along a dislocation due to the action of a stress). Only a first order approximation to the problem will be attempted here. We let L be the average length of a dislocation that might be swept out by a pair of kinks following their nucleation. L is assumed to be much larger than w, the width of the critical pair of kinks, and end effects are neglected. One possible formulation is based on the fact that there are L/b points along the length L at which a pair of kinks might be produced and consequently

$$\nu_n \simeq \nu_E \frac{L}{2b} e^{-U_n/kT} \tag{12a}$$

where ν_E is the Einstein frequency. This would apply for cases where the fluctuation might be localized. On the other hand when the thermal fluctuation is spread over the critical width, say w, of the pair of kinks

$$\nu_n \simeq \frac{\nu b}{w} \frac{L}{2w} e^{-U_n/kT} \tag{12b}$$

where $\nu b/w$ is the frequency of vibration of the dislocation, ν being the Debye frequency and L/2w is approximately the number of wave lengths along the dislocation line at which nucleation might occur. These expressions differ somewhat from the original suggestions of Dorn and Rajnak (1964) (which was based partly on both concepts) that

$$\nu_n \simeq \frac{b}{w} \frac{L}{b} e^{-U_n/kT} \tag{12c}$$

An exact analysis for ν_n is quite complicated and perhaps not too critical at this stage. Inasmuch as the vibrations are coupled, it appears that Eq. (12b) might prove to be the more satisfactory approximation in most cases.

Eqs. (12) apply when the velocity of the kinks is so great relative to their nucleation rate that not more than one pair of kinks exist in length L at any one time. Dorn and Rajnak (1964) have also described cases where the kink velocity might be so slow relative to the nucleation rate that several pairs of kinks will be moving along a single dislocation segment at one time. Thus far, however, there have been no experimental confirmations of this possibility.

The average velocity of a dislocation moving as a result of nucleation of pairs of kinks is

$$v = \nu_n a = \frac{\nu abL}{2w^2} e^{-U_n/kT} \tag{13}$$

where Eq. (12b) is adopted, and this gives a shear-strain rate of

$$\dot{\gamma} = \rho bv = \frac{\rho L a b^2 \nu e}{2w^2} e^{-U_n/kT} \tag{14}$$

where ρ is the total length of all thermally activatable dislocation segments per unit volume of the crystal.

Unfortunately the preexponential expressions of Eqs. (13) and (14) are somewhat in doubt since w was not well-defined. This arises because the kinks of the critical pair are not abrupt. It is unlikely that $w = L$ since this would require a thermal fluctuation spread over the entire length L, an improbable event. In view of the cooperative motion of the atoms, it is much more likely that w would be several Burger's

vectors long. The maximum value that might be ascribed to w is the separation of each kink of the pair at their points of inflection. For the quasi-parabolic Peierls hill (vide Appendix I) w max is insensitive to the stress and equals about 20 - 30 b. Although these data are not available for other types of hills they are also expected to exhibit about the same values.

Verification of the Peierls mechanism has been attempted by two experimental approaches, direct determination of velocities of dislocations and macroscopic deformation experiments. In both cases it is necessary to recognize that the effective stress is $\tau^* = \tau - \tau_A$ where τ is the applied stress and τ_A an athermal stress level. Furthermore, $U_n = U_{no}\, G/G_o$, $U_k = U_{ko}\, G/G_o$ and $\tau_A = \tau_{Ao}\, G/G_o$ where G is the shear modulus of elasticity and the subscript zero refers to the absolute zero of temperature. In analyses made to date it has also been assumed, without proof, that the Peierls stress follows the same relationship, namely $\tau_p = \tau_{po}\, G/G_o$. When the shear modulus of elasticity does not change appreciably with temperature, these adjustments are of minor consequence and have been neglected.

Experiments on dislocation velocities, which will be discussed in the next section, can be compared directly with theory by means of Eq. (13). The verification of the Peierls mechanism by comparison of the dictates of Eq. (14) with data obtained from macroscopic deformation experiments, however, require several types of measurements. Typical data of τ versus T for two strain rates are illustrated in Fig. 7 where τ_{po}, τ_p, τ_{Ao}, and τ^* are identified. At $T = T_c$, $\tau^* = 0$ and $U_n = 2U_k$.

Thus for tests at a constant value of $\dot{\gamma}$, where $\frac{\rho L}{w^2}$ is assumed to be insensitive to τ and T, Eq. (14) requires that

$$\frac{U_n \, G/G_o}{2U_k \, G_c/G_o} = \frac{U_n}{2U_k} \frac{G}{G_c} = \frac{T}{T_c}$$

whence

$$U_n/2U_k = \frac{G_c T}{G T_c} = f\left(\frac{\tau^*}{\tau_p}\right) \tag{15}$$

Consequently a replot of the data in the form of τ^*/τ_p versus $G_c T/G T_c$ should agree with curves of the type given in Fig. 4. Other mechanisms, however, give somewhat similar trends and agreement on this basis alone is insufficient to confirm the Peierls mechanism.

A more critical judgement of the operation of the Peierls mechanism is obtained from the experimentally determined activation volume which is defined by

$$v_a = kT \left(\frac{\partial \ell n \dot{\gamma}}{\partial \tau^*}\right)_T \tag{16}$$

For the Peierls mechanism (Eq. (14)) this becomes

$$v_a = kT \left(\frac{\partial \ell n \rho}{\partial \tau^*}\right)_T - 2kT \left(\frac{\partial \ell n w}{\partial \tau^*}\right)_T + v^* \tag{17}$$

where v^* (Eq. (11a)) can be rewritten as

$$v^* = - \frac{2U_{ko}}{\tau_{po}} \frac{\partial\left(\frac{U_n}{2U_k}\right)}{\partial\left(\frac{\tau^*}{\tau_p}\right)} \tag{18}$$

The remaining unknown needed to evaluate v*, namely U_{ko}, can be obtained from T_{c1} and T_{c2} for two different strain rates. Assuming $\rho L/w^2$ of Eq. (14) is insensitive to changes in temperature, namely

$$\dot{\gamma}_1/\dot{\gamma}_2 = \frac{e^{-\frac{2U_{ko}\, G_1/G_0}{kT_{c1}}}}{e^{-\frac{2U_{ko}\, G_2/G_0}{kT_{c2}}}}$$

Introducing the value of $2U_{ko}$ so obtained permits the evaluation of v* (Eq. (11)). Thus far, data that suggest the Peierls mechanism, confirm that $v_a \simeq v^*$, revealing that $\frac{\partial \ell n \rho L/w^2}{\partial \tau^*}$ of Eq. (17) is negligibly small. Consequently, when the Peierls mechanism is operative, v_a closely follows the trends of v*. This can be easily checked by plotting the experimental values of $\frac{v_a \tau_{po}}{2U_{ko}}$ versus τ^*/τ_p to compare with the corresponding theoretical curves of $v^*\tau_p/2U_k$ versus τ^*/τ_p given in Fig. 6.

Although considerable emphasis has been ascribed to the use of apparent activation energies, it must be admitted that they are not very good for identification of the Peierls mechanism. As shown by Eq. (14), the free energy for nucleation of pairs of kinks increases linearly with the temperature according to

$$U_n = kT\, n\, \frac{\rho L a b^2 \nu}{2w^2 \dot{\gamma}} \qquad (19)$$

for constant strain rate tests. Three somewhat different apparent activation energies have been defined, namely

$$q_\tau = \left(\frac{\partial \ell n \dot{\gamma}}{\partial -\frac{1}{kT}}\right)_\tau \tag{20a}$$

$$q_{\tau^*} = \left(\frac{\partial \ell n \dot{\gamma}}{\partial -\frac{1}{kT}}\right)_{\tau^*} \tag{20b}$$

and

$$q_{\left(\frac{\tau^*}{\tau_p}\right)} = \left(\frac{\partial \ell n \dot{\gamma}}{\partial -\frac{1}{kT}}\right)_{\left(\frac{\tau^*}{\tau_p}\right)} \tag{20c}$$

None are limited exclusively to the Peierls mechanism. The first is applied to either creep tests or tension tests directly on the raw data of $\tau \equiv \tau(\dot{\gamma},T)$ for a given state whereas in the last case the data are first reduced in terms of the shear modulus of elasticity. The results differ because in Eq. (20a) τ is held constant, in Eq. (20b) $\tau^* = \tau - \tau_A$ is constant whereas in Eq. (20c) $\tau^*/\tau_p = (\tau - \tau_A)/\tau_p$ is held constant. It is easily shown that for case (20c)

$$q_{\left(\frac{\tau^*}{\tau_p}\right)} = G_o U_n / G \tag{21}$$

which causes $q_{(\tau^*/\tau_p)}$ to increase slightly more rapidly than linearly with T for constant strain-rate tests. However, all other thermally activated low temperature mechanisms give about the same trends with temperature and differ only relative to the sensitivity of the appropriate logarithmic

term of Eq. (20) to the stress and temperature. Alternately U_n from (21) might be plotted as a function of τ^* or of τ^*/τ_p but the trends so obtained, are more readily and more accurately given by Eq. (15).

Two additional confirmations of the Peierls theory, however, are significant: (a) a reasonably correct line energy of about $\Gamma_o \approx Gb^2/2$ should be obtained from Fig. 3 when the experimentally determined values of τ_p and U_k are employed; (b) the preexponential term of Eq. (14) should give reasonable values of $\rho L/w^2$.

IV. COMPARISON WITH EXPERIMENTAL DATA

In this section the Peierls theory will be correlated with experimental results on the plastic deformation of some ionic solids, metals, alloys and covalent solids.

A. Ionic Crystals

As mentioned in the introduction we might expect high Peierls stresses in ionic crystals.

Thomson and Roberts (1960), May and Kronberg (1963), Hulse et al. (1963) and Copley and Pask (1965) have studied the temperature dependence of plastic yield stress of single crystals of MgO. A large difference in dislocation mobility is probably responsible for the differences in the observed yield stress for the motion of <110> dislocations on the {100} and the {110} glide planes. As pointed out by Huntington et al. (1955) and Gilman (1959), higher core energies and anion closed shell repulsions could explain the more difficult glide in {100} plane. This feature and the rapid decrease in yield stress with increase in temperature are consistent with the Peierls process. The {100} Peierls

stress, yield stress at 0°K, Copley and Pask (1965), suggests, according to Eq. (6a), a not unreasonable kink energy of 0.18 eV.

Several data, however, seem to disqualify the Peierls mechanism; for example the {100}<110> yield stress decreases almost linearly with increasing T in contrast to the expected trends (vide Fig. 4) for the Peierls process. Activation volumes deduced from the results of May and Kronberg (1963) exhibit high scatter from crystal to crystal; and the variation of the average values of v_a with temperature from 20 to 100 b^3 at room temperature to excessively large values near T_c are at variance with expectations based on the Peierls mechanism.

LiF also exhibits anisotropy relative to yield stress for {100} and {110} glide, the {100} being more difficult, Gilman (1959). Using as critical temperature T_c (≈700°K for {100} slip), the kink energy can be estimated (Eq. (14)) from

$$U_k \simeq \frac{kT_c}{2} \ln \left(\frac{\rho a b^2 \nu L}{2w^2 \dot{\gamma}}\right) \qquad (16)$$

Taking reasonable values for $\rho = L^{-2} = 10^6/cm^2$, $w = 30$ b, we get U_k = 0.75 eV, and from (8a) assuming $\Gamma_o = Gb^2/2$ we deduce a Peierls stress to be about 200 kg/mm^2; the value obtained from the extrapolation of τ to 0°K is, however, much lower than this (≈6 kg/mm^2). Apparently the Peierls process does not control here.

Furthermore, the measurements by Johnston and Gilman (1959) of the velocities of dislocations in LiF as obtained by etching techniques does not agree with Eq. (13). Below about 10^{-1}cm/sec they found that, between -50°C and 25°C, the velocity varies

as $v \propto \tau^m \exp(-E/kT)$ where τ is the applied stress, m ranges from 15 to 25, varying slowly with temperature, and E is supposedly an activation energy that is independent of the stress. Such results are incompatible with Eq. (13) where U_n is very sensitive to the stress; it is also unlikely that the preexponential term in Eq. (13) can vary as steeply as the 15th to 25th power of τ for the Peirls process.

Johnston and Gilman noticed that the resistance to dislocation motion and the initial yield stress of LiF were affected by the impurities and radiation damage effects. This point has been further emphasized by Johnston (1962). Whereas the shear stress of quite pure single crystals decreases slowly with test temperature, the shear stress of impure crystals is much higher and decreases exponentially with temperature. Divalent impurities (such 80 p.p.m. of Mg^{2+}) strongly influence the flow stress, perhaps because the tetragonal lattice distortions due to Mg^{2+} + Li^+ vacancy pairs (Fleisher (1962)); certain effects, however, are inexplicable in terms of this latter theory, Dryden et al. (1965), Nadeau (1966). Although no theory is available to accurately account for the effects of impurities or radiation damage in LiF it can be concluded that the Peierls mechanism does not control the plastic deformation of ionic crystals of usual purity and that their Peierls stress is probably smaller than that required for activation of dislocations past tetragonal strain centers.

B. B.C.C. Metals

The plastic deformation at low temperatures of b.c.c. transition metals (V, Nb, Ta, Cr, Mo, W and Fe) has been subjected to detailed

studies during recent years. The possible validity of the Peierls theory has been extensively tested by Conrad (1963), Dorn and Rajnak (1964) and Christian and Masters (1964).

Obviously preexisting kinks in dislocations inclined with respect to close-packed directions move at small applied stresses giving microdeformations. Experiments by Brown and Ekvall (1962) and more recently by Kossowsky and Brown (1966) on microyielding in iron might be interpreted in this way. As will be discussed later, however, Escaig (1966) has suggested an alternate explanation of such microyielding and initial strain hardening. We will deal here only with macrodeformation, i.e. with the macroscopic yield or flow stress.

Two kinds of comparison will be made. The first consists of comparing the experimental dependence of the flow stress on temperature with the theoretical ones given in Fig. 4. The second consists of comparing the experimentally determined activation energies and activation volumes with the theoretical values subject to the restrictions mentioned in paragraph III_B. Such plots made by Dorn and Rajnak (1964) from the experimental results summarized by Conrad (1963), usually show good agreement between theory and experiment for the above-mentioned metals. We emphasize here only the new results obtained on single crystals of Mo and Ta (Lau et al. (1966)) and later those on polycrystalline iron 2wt% manganese alloy with various amounts of interstitial impurities, (Wynblatt and Dorn (1965)) and on polycrystalline Fe - 11 at.% Mo, (Rawlings and Newey (1966)).

Figure 8 shows the variations of the thermal stress τ^* as a function

of temperature T for the (110) glide of Ta and Mo, by using reduced coordinates τ^*/τ_p and T/T_c; the lines refer to the theory for three values of α (vide Fig. 4). Since the most distinctive characteristic of the Peierls mechanism is its small activation volume we have also plotted in Fig. 9 the experimentally determined activation volume v_a, the experimentally deduced activation volume $v_e^* = -(\partial U_n/\partial \tau^*)_T$ where U_n is the experimentally determined activation energy, and v^* the theoretical activation volume as deduced from previously determined values of $2U_k$ and τ_p. In all cases agreement is excellent illustrating that the low temperature deformation of Mo and Ta most likely occurs by the Peierls mechanism. Furthermore the good coincidence of the v_a and v_e^* with the said line v^* curves demand that, as suggested by theory, $\rho L/w^2$ is practically independent of the stress.

The data for Fe-2 wt.% Mn of different purities (Wynblatt and Dorn (1965)), Fig. 10, appear to coincide with the dictates of the Peierls theory only over the range of $T/T_c < 0.7$. Almost identical trends have been observed for Fe - 11 at.% Mo by Rawlings and Newey (1966). Furthermore for $T/T_c > 0.7$ or $\tau^*/\tau_p < 0.1$ the activation volumes, Fig. 11, increase much more rapidly with decreasing stress, cf. also Ohr (1966), than is permissible by the Peierls mechanism. On the other hand the values of v_a for $T/T_c < 0.7$ or $\tau^*/\tau_p > 0.1$ are in reasonable agreement with expectations based on the Peierls mechanism. The anomalously low values of v_e^* are probably due to errors introduced in estimating U_n as a function

of τ^*/τ_p from the original data and cannot therefore be used to estimate how the preexponential term of Eq. (14) might vary with stress. The activation volume, as well as τ^* are independent of the level of interstitial impurities, Wynblatt and Dorn (1965), Keh (1965). In contradiction with the results obtained by Stein et al. (1963), they appear only to affect the athermal stress. Impurities could influence the effective stress τ^* in one or more of four ways: (a) they could modify the Peierls stress; (b) the impurities could require the operation of a different thermally activated mechanism, Friedel (1963); (c) impurities could pin-down the dislocation line, modifying the expansion of the kinks by affecting L and w, as qualitatively considered by Kossowsky and Brown (1966); (d) a mixture of (b) and (c) could become operative, Celli et al. (1963).

Although the situation is complex, the present results suggest, as was also pointed out by Conrad (1963), that interstitial impurities and solute atoms only affect the long-range athermal stresses in Fe. Another point in favor of the Peierls mechanism is the invariance of the activation volume with strain or prestrain, Lau et al. (1966), Wynblatt and Dorn (1965).

We give finally in Table 1 some characteristic values of these three metals deduced from the analyses in terms of the Peierls mechanism:

(a) Peierls stress at zero degrees Kelvin, τ_p^o. Deduced by extrapolation to zero degree of the shear stress or by more sophisticated comparison between experiment and theory Lau et al. (1966);

(b) Kink energy U_k. Obtained from the values of the critical temperature T_c (where $\tau^* = 0$) at two strain rates;

(c) Line energy Γ_o. Deduced from τ_p^o and U_k by using Fig. 3;

(d) Critical width of a double kink w. The preceeding analysis showed that w does not vary very much with the stress and so w is calculated by using (A.1.10) which is valid at low stresses.;

(e) Upper and lower bound values of densities of dislocations. From Eq. (14) the preexponential term can be estimated by plotting the activation energy U_n versus temperature. The density ρ is obtained by assigning reasonable values to L. L is taken to be between the size of the Frank network, i.e. $\rho^{-1/2}$, and the critical double kink width w; the corresponding limit values of ρ are deduced.

The values in Table 1 have reasonable orders of magnitude except for the fact that the densities of dislocations in Mo and Fe-Mn, are somewhat too high for the small prestrain used in determining the flow stress; a rough estimate of the density of dislocations might be made from the long range athermal stress τ_A which is related to the density of dislocations, at least for an homogeneous distribution of dislocations by the relation $\tau_A = Gb/\beta\rho^{-1/2}$, where β is a constant equal, in b.c.c. structure, to about 4, Saada (1963). Such a relation suggests densities of the order of a few $10^8/cm^2$ which are more reasonable. The preexponential term of Eq. (14) however is too crude to discard the Peierls mechanism exclusively on this basis alone. Thus it appears that

the Peierls mechanism explains fairly well the flow stress of b.c.c. metals at low temperatures for plastic strains large enough to displace preexisting kinks and thus array dislocations along close-packed rows of atoms.

A competitive mechanism for explaining the deformation of b.c.c. metals at low temperatures is that due to the recombination of sessile dissociated screw dislocations, Escaig (1966). This model assumes that during the microdeformation screw dislocations of the type 1/2 [111] are formed, and they are stabilized by splitting on several planes (110), Kroupa (1963), or [112], Hirsch (1960), Sleeswyk (1963). The sessile barriers so introduced can be eliminated by thermally activated recombination on one of the dissociation planes. On this basis Escaig calculated the temperature dependence of the macroscopic elastic limit. Fitting the theoretical curve with experiment for high purity b.c.c. metals he deduced the stacking fault energy in (110) or (112) planes. The energies so obtained are typically of the order of Gb/100, corresponding to dissociations of only several interatomic distances.

Two points disqualify the use of this theory to predict the flow-stress temperature variations of b.c.c. metals over the whole range of low temperatures (i.e. from 0^{o} K to T_c):

(a) As mentioned by Escaig himself, the theoretical $\tau^* - T$ curves for the recombination mechanism decrease more rapidly over the lowest temperature range than is obtained experimentally. Thus when theory and experiment are adjusted to agree over the intermediate ranges of temperature, the theory requires

a flow stress τ_o at the absolute zero, that is about four times that suggested by extrapolating the experimental data;

(b) The stacking fault energies deduced from the theoretically estimated τ_o, namely $\gamma \simeq 10^{-2} Gb$, then suggest that the partial dislocations remain in glissile configuration on a single plane since the condition for dissociation into sessile dislocations on three different planes is that $\gamma < 0.7 \times 10^{-2} Gb$.

Condition (a) suggests that the recombination mechanism is inconsistent with experimental results on b.c.c. metals at the lowest temperatures. For iron, the Peierls process satisfies the experiment much better than the recombination at high stress, i.e. below about 170°K. As previously mentioned, above this temperature the Peierls mechanism can no longer explain either the temperature dependence of the flow stress or the apparent activation volumes. And as will be shown, precisely in this range of low stresses the mechanisms based on the recombination of screw dislocations is satisfactory.

We successively compare with experiment the flow stress τ^*, activation energy U, activation volume v^* given by the expressions (17), (18), (19).

At low stresses where $\tau^* << \tau_o$, according to Escaig,

$$\tau^* = \frac{1}{150} \frac{G\, b^3}{kC} \left\{-\left[15 \frac{\tau_o}{G} + \ell n \left(1 - 15 \frac{\tau_o}{G}\right)\right]\right\}^{3/2} \times \frac{1}{T} \qquad (17)$$

where C is approximately a constant equal to 45.

$$U = \frac{1}{150} G^2 b^3 \left\{-\left[15 \frac{\tau_o}{G} + \ell n \left(1-15 \frac{\tau_o}{G}\right)\right]\right\}^{3/2} \times \frac{1}{\tau^*} \qquad (18)$$

$$v^* = -\left(\frac{\partial U}{\partial \tau^*}\right)_T \simeq 8\, b^3 \frac{\tau_o^3}{G} \times \frac{1}{\tau^{*2}} \qquad (19a)$$

The apparent activation volume v_a can be written,

$$v_a = kT\left(\frac{\partial \ell n \dot{\gamma}}{\partial \tau^*}\right)_T = \frac{2kT}{\tau^*} + v^* \qquad (19b)$$

The experimental plots of τ versus $1/T$, U versus $1/\tau^*$, v^* versus $1/\tau^{*2}$ are shown in Figs. 12, 13 and 14. The plots fit well the previous relations:

(a) Flow stress. By extrapolation to zero $1/T$ we deduce an athermal stress τ_i of 2.3 and 2.6 kg/mm^2 for the two grades of purity. A change in mechanism is noted at about 220°K. Below this temperature (where the Peierls process agrees with experiment) an almost linear dependence of τ versus $1/T$ seems to be observed;

(b) Activation energy. Above about 220°K, the activation energy varies linearly with $1/\tau^* = 1/(\tau-\tau_i)$. The critical temperature T_I for τ as for U, is also about 220°K, i.e. higher than T_I given by plotting τ or U versus T and comparing with the theoretical curves of the Peierls theory (≈170°K, as mentioned previously);

(c) Activation volume. The real v^* and apparent v_a activation volumes vary in the range of low stresses, as $1/\tau^{*2} = 1/(\tau-\tau_i)^2$.

From the slopes of the different plots, τ_o is deduced using (17), (18) and (19a). The stacking fault energy γ is calculated from τ_o after

the Escaig relation

$$\tau_o/G_o = 4.25\ (1/63 - \gamma/G_o b).$$

We successively obtained the internally consistent results of γ = 220, 230 and 230 ergs/cm^2 from the three methods. Since the tests were conducted on polycrystalline iron, probably both (110) and (112) planes were operative. Although Eqs. (17), (18) and (19) refer to the splitting on (110) planes, Escaig showed that similar variations of τ, U and v* will be obtained when the stacking fault energies on (110) and (112) planes are about the same. Thus γ here represents a mean stacking fault energy, close to the average for all planes.

On the other hand, the high value deduced for τ_o, between 130 and 160 kg/mm^2, disqualifies this mechanism below the critical temperature T_I (vide Fig. 12); the extrapolation to 0°K of the flow stress by the recombination mechanism should have been about ≈45 kg/mm^2 (cf. Table 1).

The temperature dependence of the flow stress of iron seems well explained by the Peierls process from 0°K to about T_I ≈ 200°K and by the recombination mechanism above this temperature. In the range of the high temperatures the stress for recombination of the partials of screw dislocations, varies less steeply with temperature, becomes higher than the Peierls stress, and therefore will control the deformation. Below T_I, the Peierls stress is the higher and the partials once recombined need only to overcome this frictional stress to move; besides, the edge dislocations are probably perfectly glissile and also contribute to the deformation through the Peierls mechanism.

The observations of Keh and Weissman (1963) by electron microscopy on deformed polycrystalline iron are in agreement with the previous predictions: at low temperatures the dislocations are uniformly distributed, lying on crystallographic planes and relatively straight, as can be expected from a Peierls process. At higher temperature, depending on the strain, a cell structure appears. Although the process of cell formation is not well explained, the incidence of cross slip of recombined screw dislocations, without further limitations by a Peierls process, might account for such cell formation at high temperature.

The same sequence of mechanisms does not appear to occur in molybdenum and tantalum; the Peierls mechanism does agree with the tests over the whole thermal range. A higher stacking fault energy for this metal might lower the cross slip stress such that the Peierls process remains relevant. Furthermore, screw dislocations are observed to lie along [111] directions, Lawley and Gaiger (1964) for Mo and Arsenault (1966) for Ta, suggesting that the Peierls stress is higher for the screw than for the edge dislocations. The observation of cell structure formation at high strains in both Mo, and Ta at room temperature, Keh and Weissman (1963), suggest too that the recombination stress of split screw dislocations becomes of the same order of magnitude as that needed to initiate the Peierls mechanism causing the recombination mechanism to also become operative.

IV_3. Some Alloys.

The low temperature deformation for some alloys can be rationalized

in terms of the Peierls mechanism. We summarize here some results obtained on the prismatic slip $(\bar{1}100)[11\bar{2}0]$ of the short range ordered Ag_2Al, Rosen et al. (1964) Mg-Li alloys Ahmadieh et al. (1965), the $(\bar{3}21)$ [111] slip in long range ordered AgMg (CsCl type structure), Mukherjee et al. (1965).

The rapid increase in the flow stress at low temperature, the activation energy and the activation volume are again in agreement with the Peierls model. The data deduced by similar analysis as that previously given for b.c.c. metals are shown in Table 2.

Some remarks can be made: (1) for Mg-Li alloys, the lithium additions appear to lower the Peierls stress and therefore the low temperature shear stress for prismatic slip. Similar softening of some b.c.c. solid solutions has also been described, Arsenault (1966). With our interpretation in terms of the Peierls mechanism, the theoretical explanation of this softening has to be found in the change in the electronic structure of the alloy with lithium additions; (2) the range of deduced dislocation densities is wider than for the b.c.c. metals above analyzed. As previously mentioned, the action of impurities is complex; nevertheless pinning of dislocations along the close packed rows by impurity atoms might reduce L and in this way suggest intermediate values of ρ. Besides, the values of ρ^* are here more reasonable than these of ρ^+, to the contrary of the b.c.c. metals.

The observation by Okamoto (1966) of straight screw $[11\bar{2}0]$

dislocations in the prismatic plane of Ag-Al is in agreement with the Peierls mechanism.

IV_4. COVALENT METALS

As mentioned in the introduction, a strong Peierls energy is expected in covalent metals, like germanium and silicon. Furthermore, mobile dislocations running parallel to close-packed rows have been observed by electron microscopy. Actually different authors have speculated on the kink nucleation and kink migration as the controlling mechanism of these metals, Celli et al. (1963), Susuki (1963), Holt and Dangor (1963). Recent calculations made by Labusch (1964) found good agreement between the experimental activation energy and the energy of generation of a pair of kinks, showing that only one pair of kinks at a time is nucleated along the whole length of the dislocation segments.

On the other hand, Haasen (1957) (1963) (1964) developed a cracked core model, where the Peierls force originates from the breaking of bonds when the dislocation moves in the slip plane; a linear stress dependence of the dislocation velocity is expected from this model, in fair agreement with experiment.

Since Haasen's talk deals during this congress with this subject we shall discuss this aspect no further.

V. CONCLUSION

1. The continuum line-energy model for estimating the free energy of activation needed to nucleate a pair of kinks in terms of the kink energy, Peierls stress, and effective stress is now fairly well established.

2. Several details of formulating the effect of stress, and temperature on the strain rate, however, require further investigation. These are concerned with the following issues:

(a) The determination of actual shapes of Peierls hills and magnitude of the Peierls stresses in terms of atomic potentials or quantum theory.

(b) A more accurate formulation of the preexponential term in the strain rate expression.

(c) A more complete statistical treatment of the model.

(d) Introduction of effects arising from solute atoms and interstitial impurities.

3. The low temperature thermally activated deformation of a number of metals and alloys agrees well with the dictates of the Peierls mechanism. These are 1/2[111]{110} slip in single crystals of Mo and Ta, 1/2[111]{123} slip in single crystals of AgMg, 1/3 $[11\bar{2}0]\{1\bar{1}00\}$ slip in Ag + 33 at.% Al, and in Mg with 6 to 12 at.% Li, deformation in polycrystalline Fe plus 2 wt.% Mn with various degrees of interstitial purity and Fe plus 11 at.% Mo at temperatures below 170°K. (Between 170° and 400°K the thermally activated mechanism for deformation of the polycrystalline Fe alloys agree with Escaig's model based on recombination of dissociated dislocations.) Evidence suggests that some Group 4 metals also obey

the Peierls mechanism. Although ionic crystals are expected theoretically to deform at low temperatures by the Peierls mechanism, experimental results suggest that their thermally activated mechanism is controlled by some other process which is sensitive to impurity concentrations.

4. The major advance to be made concerns replacement of the continuum-type line-energy model for nucleation of pairs of kinks by a more realistic atomic model.

APPENDIX 1

"Quasi-Parabolic" Peierls Hills

Various authors, Seeger (1956), Friedel (1964), supposed that the dislocation remained at y = -a/2, i.e. at the bottom of the Peierls hill, independently of the level of the applied stress. With sinusoidal hills such assumption is approximated only at low stresses. For quasi-parabolic hills, as shown in Fig. 2d, however, dislocations remain at y = -a/2 for all possible stresses up to the Peierls stress. Assuming a line energy of

$$\Gamma(y) = \Gamma_o^{1/2} \left[\Gamma_o + \frac{ab\tau_p}{2}\left(1 - \frac{4y^2}{a^2}\right)\right]^{1/2} \qquad (A.1.1)$$

the problem of nucleation of pairs of kinks can be completely solved analytically. Introducing expression A.1.1 of $\Gamma(y)$ into Eq. (3), gives

$$U_n = 2 \int_{-a/2}^{y_c} [qy^2 + ry + s]^{1/2}\, dy \qquad (A.1.2)$$

where $q = -\tau^{*2}b^2 - 2b\tau_p \frac{\Gamma_o}{a}$

$$r = -\tau^{*2}b^2 a - 2\tau^* b\Gamma_o$$

$$s = \frac{ab\tau_p\Gamma_o}{2} - \tau^* \frac{b^2a^2}{4} - \tau^* ba\Gamma_o$$

and $-\frac{a}{2}$ and y_c are the roots of $qy^2 + ry + s$. The integration of (A.1.2) finally gives:

$$U_n = \frac{b^2\Gamma_o^{\,2}(\tau_p - \tau^*)^2\pi}{\left(\frac{2b\tau_p\Gamma_o}{a} + \tau^{*2}b^2\right)^{3/2}} \qquad (A.1.3)$$

$$\simeq (1-\tau^*/\tau_p)^2 \, \pi a \sqrt{\frac{ab\tau_p \Gamma_o}{8}} \qquad (A.1.4)$$

Similarly from (4) the energy of a kink is

$$U_k = \frac{\pi a}{4} \sqrt{\frac{ab\tau_p \Gamma_o}{2}} \qquad (A.1.5)$$

and from (A.1.4) and (A.1.5)

$$\frac{U_n}{2U_k} \simeq \left(1 - \frac{\tau^*}{\tau_p}\right)^2 \qquad (A.1.6)$$

In Fig. 4 is shown a plot of $\frac{U_n}{2U_k}$ as a function of τ^*/τ_p and also the plots for sinusoidal hills where $-1 \leq \alpha \leq 1$. All curves are practically identical at low stresses. At high stress the quasiparabolic results differ, but little from those for sinusoidal hills over the range of $-1 \leq \alpha \leq 1$. We can deduce the activation volume

$$v^* = -\frac{dU_n}{d\tau^*} \simeq \left(1 - \frac{\tau^*}{\tau_p}\right) \pi a \sqrt{\frac{ab\Gamma_o}{2\tau_p}} \qquad (A.1.7)$$

$$= 2(1 - \tau^*/\tau_p) \frac{2U_k}{\tau_p}$$

which is plotted in Fig. 6, together with these for sinusoidal hills. Although the activation volume is more sensitive than $U_n/2U_k$ to the shape of the hill, on the whole the drastic changes in the shape of the hills, do not affect very much the trends.

Integration of Eq. (20) gives an analytical expression of the line

bowed into a pair of critical kinks. An approximate equation of the dislocation line is:

$$\chi = \pm \frac{\tau^* b}{\Gamma_o} \left(\frac{a\Gamma_o}{2b\tau_p}\right)^{1/2} \left[-y^2 - \frac{\tau^*}{\tau_p} ay + \frac{a^2}{4}\left(1 - \frac{2\tau^*}{\tau_p}\right) - \frac{ba^3\tau^{*2}}{8\tau_p\Gamma_o}\right]^{1/2}$$

$$\pm \left(\frac{a\Gamma_o}{2b\tau_p}\right)^{1/2} \left[\sin^{-1}\left(\frac{2\tau_p y + \tau^* a}{a(\tau_p - \tau^*)}\right) - \frac{\pi}{2}\right] \qquad (A.1.8)$$

We can also determine the width w of a critical double kink defined as the separation of the kinks at their points of inflection:

$$w = \left(\frac{a\Gamma_o}{2b\tau_p}\right)^{1/2} \left[\pi + \frac{\tau^* ba}{\tau_p \Gamma_o}\left(\tau^* - \tau_p\right)\right] \qquad (A.1.9)$$

Using reasonable numerical values for $\Gamma_o = \frac{Gob^2}{2}$ and τ_p, shows that expression (A.1.9) varies very slowly with τ^* and that w can be considered as a constant, namely

$$w = \frac{\pi}{2}\left(\frac{2a\Gamma_o}{b\tau_p}\right)^{1/2} \qquad (A.1.10)$$

The height of the kink is easily calculated too:

$$h = y_c - y_o = y_c + \frac{a}{2} = a\left(1 - \frac{\tau^*}{\tau_p}\right)$$

We deduce the interaction energy of the two kinks by applying Eq. (9), obtaining

$$U_{kk} = -\frac{\Gamma_o}{\pi^2}\sqrt{\frac{a^3 b\tau_p}{8\Gamma_o}}\left(1 - \frac{\tau^*}{\tau_p}\right)^2 \qquad (A.1.11)$$

which gives a constant ratio kink-kink energy to the energy of formation of the double kink of

$$\left|\frac{U_{kk}}{U_n}\right| = \frac{1}{\pi^3} = .03$$

The variation of the flow stress with temperature can be obtained from Eq. (14). Using (A.1.4) for U_n and (A.1.10) for w:

$$\tau^* \simeq \tau_p \left[1 - \left(\frac{T}{T_c}\right)^{1/2}\right] \qquad \text{(A.1.11)}$$

where

$$T_c = \frac{\pi a}{2}\sqrt{\frac{ab\tau_p\Gamma_o}{2}} \Big/ k \ln\left(\frac{\rho b^3 L \nu \tau_p}{\pi^2 \dot{\gamma} \Gamma_o}\right)$$

APPENDIX 2

Camels-Hump Hills

Camels-hump hills, shown in Fig. 2e, are obtained by making $\alpha > 1$ in Eq. (5a). $R = \Gamma_m/\Gamma_o$ and α are the independent variables. The kink energy under zero stress and the energy to nucleate a pair of kinks are numerically calculated by the method III_A. The details will be presented later as a letter to the editor.

Figure 3 shows a slight decrease of U_k with α; $\frac{2U_k\pi}{a\Gamma_o}$ is still very closely proportional to $\sqrt{R-1}$.

Figures A.2.1 and A.2.2 show the variation of the energy of formation of a pair of kinks and of the deduced activation volume as a function of the effective stress. The difference between the curves for $\alpha = 0$, $\alpha = \pm 1$, increase as α increases above 1. The more significant feature appears at high stresses (or low temperatures).

The curves are broken for $0.1 < \tau^*/\tau_p < 0.3$. In this range of stresses the dislocation can lie in the intermediate valley. The present data refer to the case of a single activation for surmounting the double hump. The results for $\alpha = 4$ and $R = 1.0013$ fit very closely the hill calculated by Chang (1966) in Fe for edge 1/2[111] dislocations, by using relaxation techniques. The Peierls stress is in good agreement with the experimental value ($\simeq 45$ kg/mm^2).

Table 1. Typical values for the analysis of Ta, Mo, Fe-Mn deformation in terms of the Peierls mechanism.

Metal	τ_p^o (10^8 dynes/cm^2)	U_k (eV)	$\frac{\Gamma_o}{G_o b^2/2}$	$\frac{w}{b}$	ρ^* (cm^{-2})	$\rho^\dagger$ (cm^{-2})
Ta	33.4	0.31	1.55	24	2.4×10^{8} - 2.4×10^{10}	4.1×10^{5} - 4.1×10^{7}
Mo	41.3	0.62	3	29	4.5×10^{13} - 8.9×10^{12}	5.3×10^{10} - 1.0×10^{10}
FeMn**	45	0.31	2.6	22	2.5×10^{14} - 1.4×10^{13}	4.2×10^{11} - 2.9×10^{10}
FeMo	49	0.29	1.8	17	2.5×10^{9} - 1.2×10^{10}	8.6×10^{6} - 4.1×10^{7}

*ρ was calculated by using Eq. (14).

**The values given for Fe-Mn relate to Fe-Mn, ZrH purified; for the other grades of purity the values are only slightly different

$\rho^\dagger$ was calculated assuming the frequency as given by Eq. (12a).

Table 2. Typical values for the analysis of Mg-Li, Ag Al, AgMg alloys in terms of the Peierls mechanism.

Alloy	temperature range for Peierls process	slip system	τ_p^o (10^8 dynes/cm^2)	U_K (eV)	$\frac{2\Gamma_o^*}{G_o b^2}$	$\frac{w^*}{b}$	ρ^* (cm^{-2})	$\rho^\dagger$ (cm^{-2})
Mg-10 at.% Li	0 - 300°K	prism.	7.6	0.22	4.45	29	$1.6.10^8$ - $2.7x10^4$	$1.9x10^5$ - $3.2x10^1$
Mg-12.5 at.% Li	0 - 300°K	prism.	6.8	0.21	4.54	30	$4.8x10^8$ - $2.5x10^5$	$5.3x10^5$ - $2.8x10^2$
Ag_2Al	0 - 240°K	prism.	19.3	0.19	2.09	24	$4.8x10^6$ - $2.0x10^9$	$8.3x10^3$ - $3.5x10^6$
AgMg	0 - 250°K	$(\bar{3}21)$ $[111]$	9.25	0.20	4.33**	36*	$4.8x10^3$ - $4.3x10^{7}$**	3.7 - $3.3x10^4$

*The values of Γ_o, w and ρ are obtained by using for a in the hexagonal structures a mean value $(bc)^{1/2}$ where b and c are the common lattice constants---this to taking account for the possible edge and screw character of the dislocations of Burgers vector $[11\bar{2}0]$.

**The values of Γ_o, w and ρ for AgMg refer to the screw dislocations [111] with a = 2.5b.

Figure Captions

Figure 1. Formation of a pair of kinks. a is the spacing between parallel rows of closely spaced atoms of the slip plane.

Figure 2. Line energy profiles.

Figure 3. Kink energy and Peierls' stress. R = 1.01.

Figure 4. Energy to nucleate a pair of kinks.

Figure 5. Seeger (a) and Friedel (b) models.

Figure 6. Activation volume.

Figure 7. Stress-temperature relating for the Peierls mechanism.

Figure 8. Thermal flow stress vs. temperature for (110) glide of Ta and Mo.

Figure 9. Experimental and theoretical activation volume vs. thermal flow stress for Ta and Mo.

Figure 10. Thermal flow stress vs. temperature for polycrystalline Fe-Mn of different purities.

Figure 11. Experimental and theoretical activation volume vs. thermal stress for Fe-Mn.

Figure 12. Total flow stress vs. reciprocal temperature for Fe-Mn.

Figure 13. Activation energy vs. reciprocal thermal stress for Fe-Mn.

Figure 14. Activation volume vs. $1/\tau^{*2}$ for Fe-Mn.

Figure A.2.1. Energy to nucleate a pair of kinks.

Figure A.2.2. Activation volume.

REFERENCES

Ahmadieh, A., Mitchell, J. and Dorn, J. E.: Trans. AIME 233, 1130 (1965)

Arsenault, R. J.: Acta Met. 14, 831 (1966)

Bordoni, P. G.: Ricerca Sci. 19, 851 (1949)

Brailsford, A. D.: Phys. Rev. 122, 778 (1961)

Brown, N. and Ekvall, R. A.: Acta Met. 10, 1101 (1962)

Celli, V., Kabler, M., Ninomiya, T. and Thomson, R.: Phys. Rev. 131, 58 (1963)

Chang, R.: Private communication (1966)

Conrad, H.: NPL Conf. Teddington, England (1963)

Copley, S. M. and Pask, J. A.: J. Am. Ceram. Soc. 48, 139 (1965)

Christian, J. W. and Masters, B. C.: Proc. of Roy. Soc. A281, 223 (1964)

Dorn, J. E. and Mitchell, J. B.: Report UCRL-11418 (1964)

Dorn, J. E. and Rajnak, S.: Trans. AIME, 230, 1052 (1964)

Dryden, J. S., Morimoto, S. and Cook, J. S.: Phil. Mag. 12-116, 379 (1965)

Escaig, B.: Proc. la Physique des Dislocations, Toulouse (1966)

Fleisher, R. L.: J. Appl. Phys. 33, 3504 (1962)

Frenkel, J. and Kontorova, T.: Phys. Z. Sowjetunion 13, 1 (1938)

Friedel, J.: NPL Conf. Teddington, England (1963); Dislocations, Pergamon Press (1964)

Gilman, J. J.: Acta Met. 7, 608 (1959)

Haasen, P.: Acta Met. 5, 598 (1957); NPL Conf. Teddington (1963); Discussions Far. Soc. 38, 191 (1964)

Holt D. B. and Dangor, A. E.: Phil. Mag. 8, 1921 (1963)

Hirsch, P. B.: Fifth Int. Congress of Crystallography, Cambridge (1960)

Hulse, C. O., Copley, S. M. and Pask, J. A.: J. Am. Ceram Soc. 46, 317 (1963)

Huntington, H. B., Dickey, J. E. and Thomson, R.: Phys. Rev. 100, 1117 (1955)

Jonston, W. G.: J. Appl. Phys. 33, 2050 (1962); 33, 2716 (1962)

Jonston, W. G. and Gilman, J. J.: J. Appl. Phys., 30, 129 (1959)

Jossang, T., Skylstad, K. and Lothe, J.: NPL Conf. Teddington, England (1965)

Keh, A. S.: Private communication (1965)

Keh, A. S. and Weissmann, S.: Electron Microscopy and Strength of Crystals, John Wiley and Sons (1963)

Kossowsky, R. and Brown, N.: Acta Met. 14, 131 (1966)

Kroupa, F. and Brown, L. M.: Phil. Mag., 6, 1267 (1961)

Kroupa, F.: Phys. Stat. Sol. 3, K391, (1963)

Labush, R.: Discussions Far. Soc. 38, 273 (1966)

Lang, A. R.: J. Appl. Phys. 29, 597 (1958)

Lau, S. et al.: Report UCRL-16601 (1966)

Lawley, A. and Gaigher, H. L.: Phil. Mag. 10, 15 (1964)

Lothe, J. and Hirth, J. P.: Phys. Rev. 115, 543 (1959)

May, J. E. and Kronberg, M. L.: J. Am. Ceram. Soc. 43, 525 (1963)

Mukherjee, A. K. et al.: Report UCRL-16433 (1965)

Nabarro, F. R. N.: Adv. Phys. 1, 271 (1952)

Nadeau, J. G.: Private communication (1966)

Ohr, S. M.: Report ORNL-3949, 26 (1966)

Okamoto, P. A.: Private communication (1966)

Peierls, R.: Proc. Phys. Soc. 52, 34 (1940)

Rawlings, R. and Newey, C.: to be published in Acta Met.

Rosen, A., Mote, J. D. and Dorn, J. E.: Trans. AIME 230, 1070 (1966)

Saada, G.: Electron Microscopy and Strength of Crystals, John Wiley and Sons (1963)

Seeger, A.: Phil. Mag. 1, 651 (1956)

Seeger, A., Donth, H. and Pfaff, F.: Discussions Far. Soc. 23, 19 (1957)

Seitz, F.: Adv. Phys. 1, 43 (1952); Phys. Rev. 88, 722 (1952)

Sleeswyk, A. W.: Phil. Mag. 8, 1467 (1963)

Stein, D. F., Low, J. R. and Seybolt, A. V.: Acta Met. 11, 125 (1963)

Suzuki, H.: Symp. J. of the Phys. Soc. of Japan 18, 182 (1963)

Thomson, D. S. and Roberts, J. P.: J. Appl. Phys. 31, 433 (1960)

Wallace, J., Nunes, A. C. and Dorn, J. E.: Acta Met. 13, 375 (1965)

Wynblatt, P. and Dorn, J. E.: Report UCRL-16601 (1965)

ACKNOWLEDGEMENT

This research was conducted as part of the Inorganic Materials Research Division of the Lawrence Radiation Laboratory, Berkeley. The authors express their appreciation to the United States Atomic Energy Commission for their support of this effort. They thank Mr. J. Wallace for the numerical calculations.

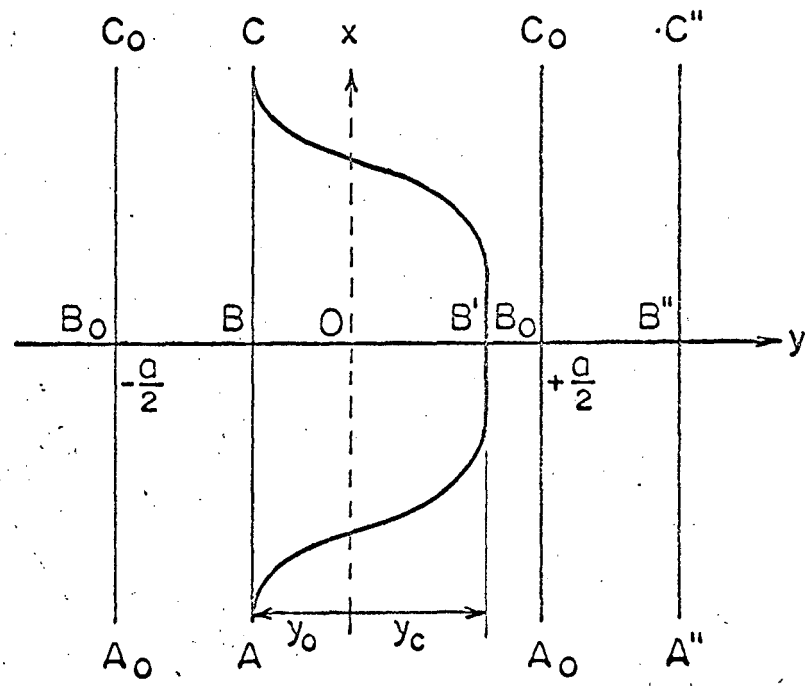

Fig. 1

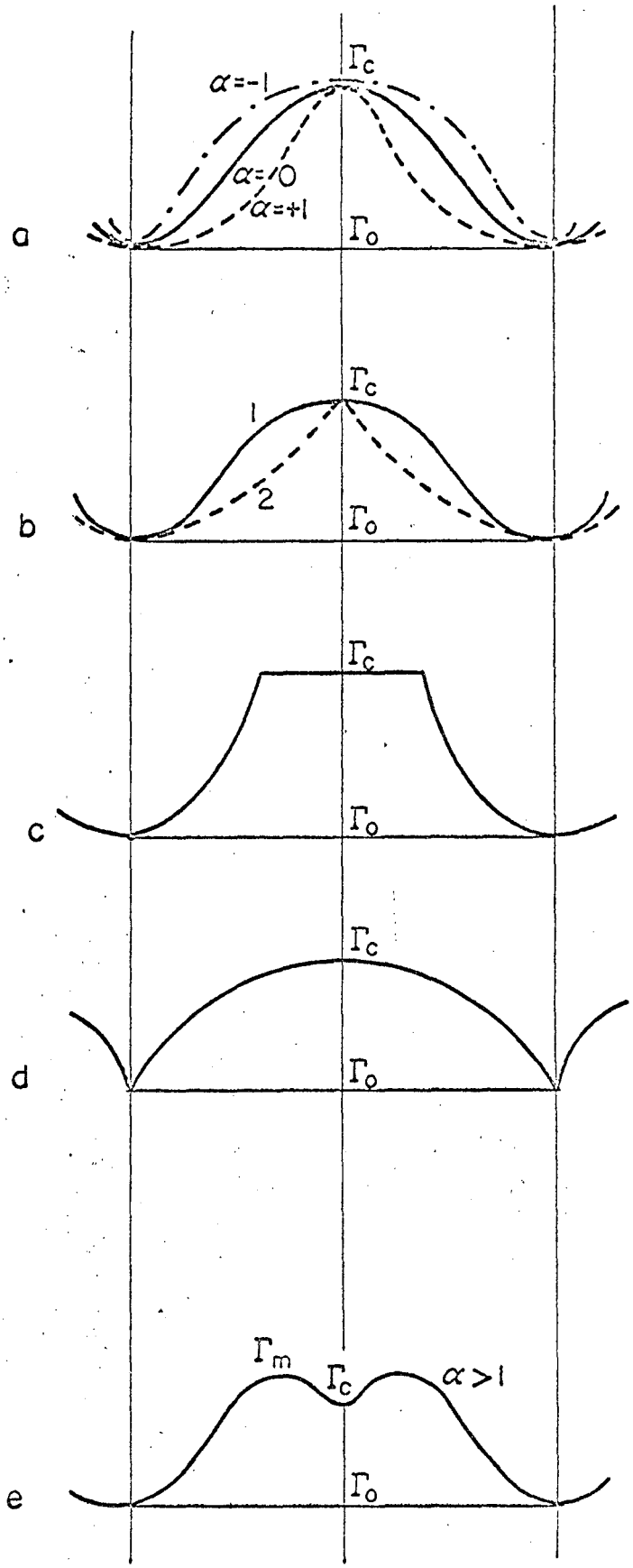
a
Γ_c
$\alpha=-1$
$\alpha=0$
$\alpha=+1$
Γ_o
b
Γ_c
1
2
Γ_o
c
Γ_c
Γ_o
d
Γ_c
Γ_o
e
Γ_m
Γ_c
$\alpha>1$
Γ_o

Fig. 2

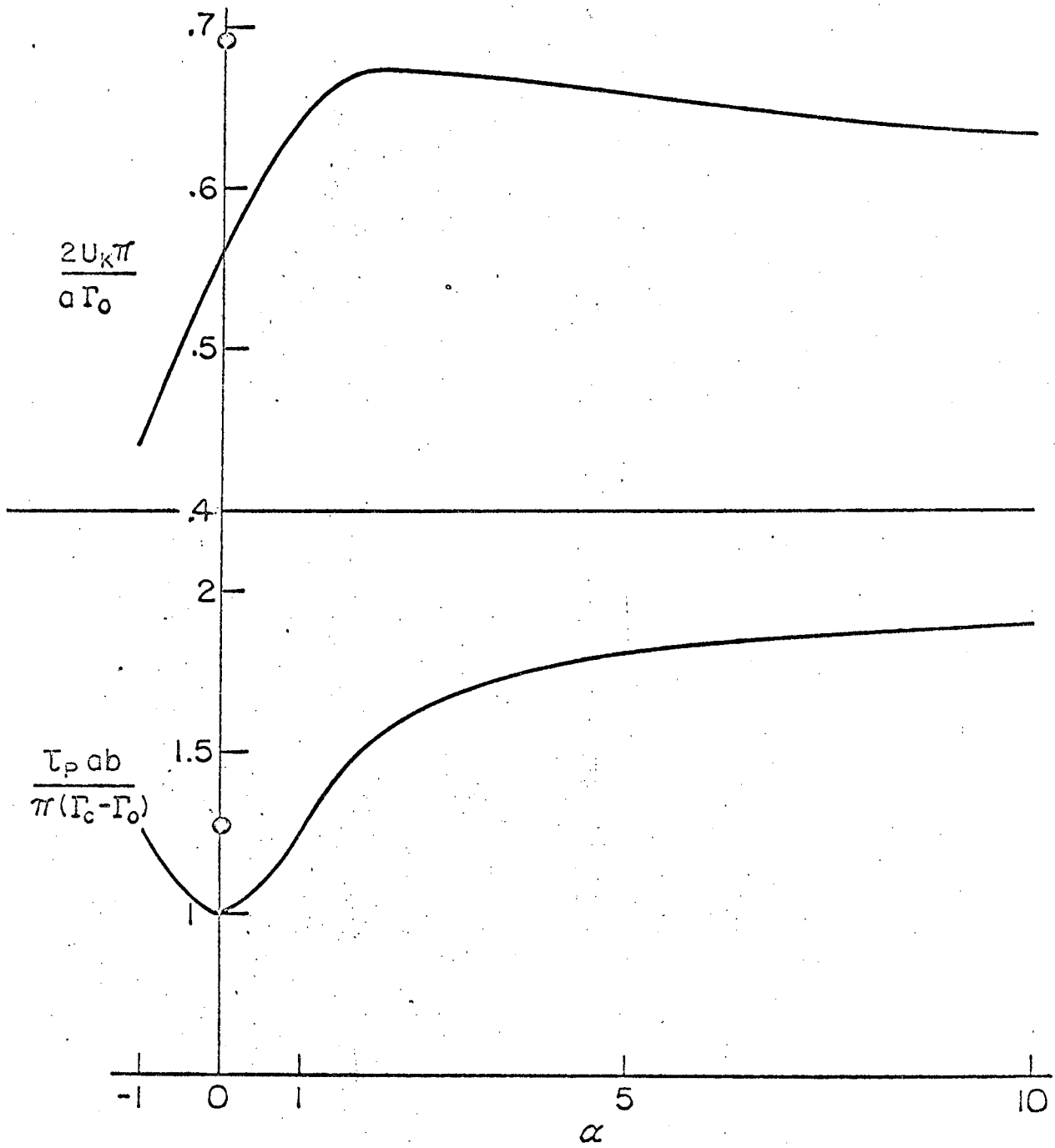
.7
.6
.5
.4
$\frac{2U_K\pi}{a\Gamma_0}$
2
1.5
1
$\frac{\Gamma_p ab}{\pi(\Gamma_c-\Gamma_0)}$
-1
0
1
5
10
α

Fig. 3

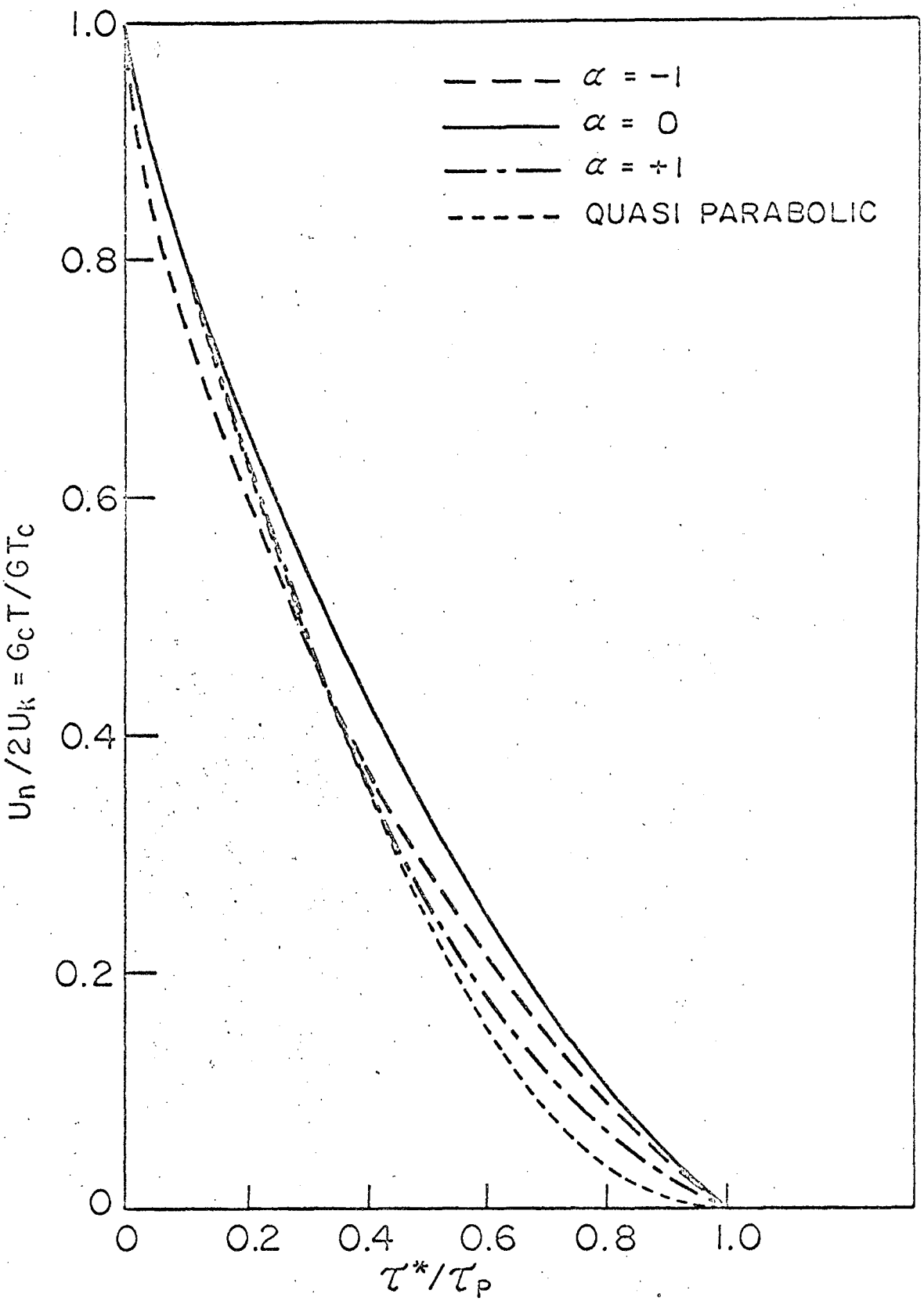
1.0
0.8
0.6
0.4
0.2
0
0
0.2
0.4
0.6
0.8
1.0
$U_n/2U_k = G_c T/GT_c$
τ^*/τ_p
$\alpha = -1$
$\alpha = 0$
$\alpha = +1$
QUASI PARABOLIC

Fig. 4

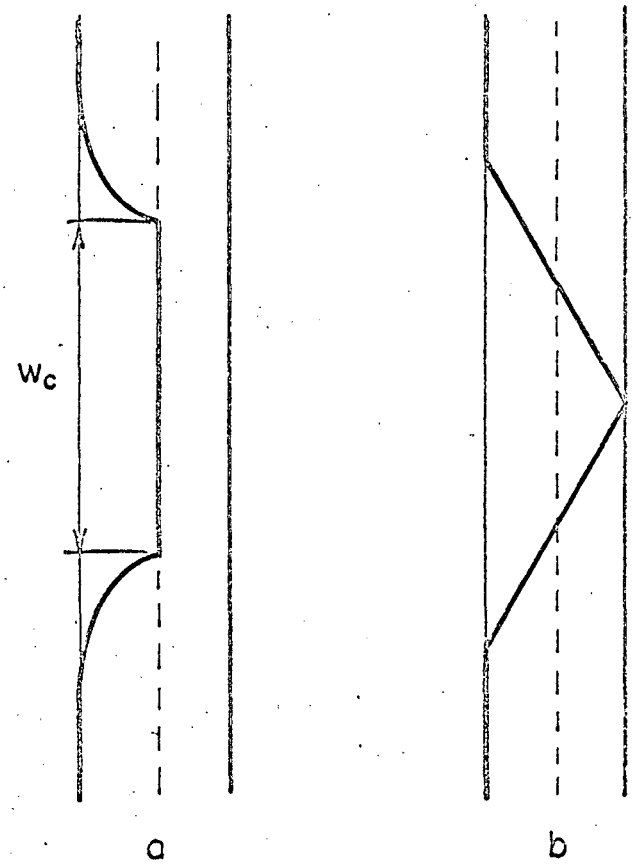

Fig. 5

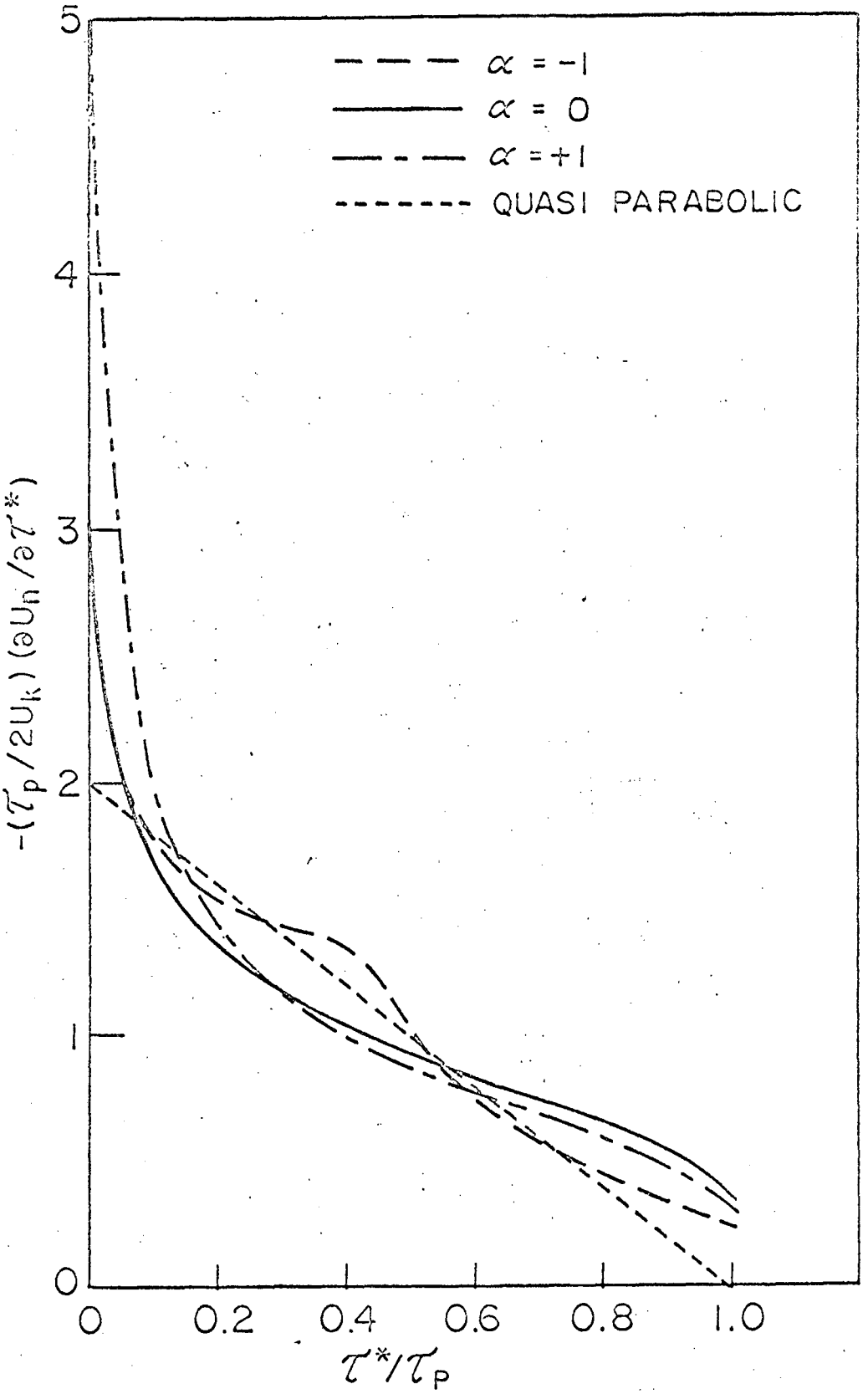
α = -1
α = 0
α = +1
QUASI PARABOLIC
$-(\tau_p/2U_k)(\partial U_h/\partial \tau^*)$
τ^*/τ_p
0
1
2
3
4
5
0
0.2
0.4
0.6
0.8
1.0

Fig. 6

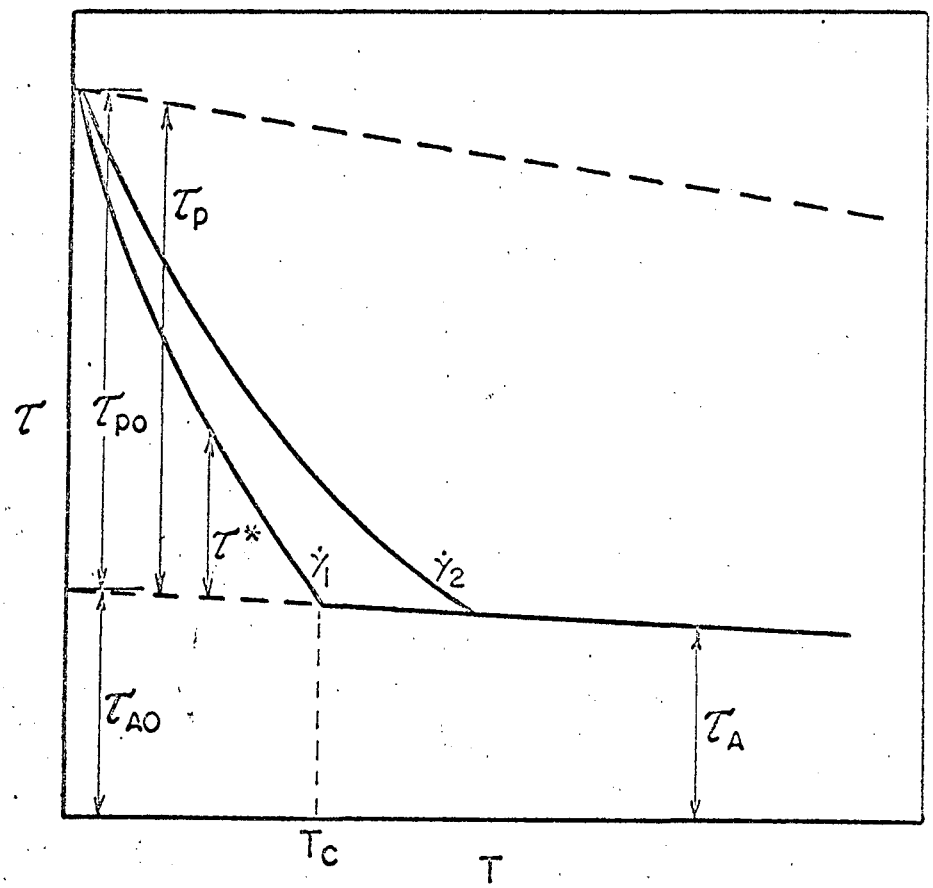

Fig. 7

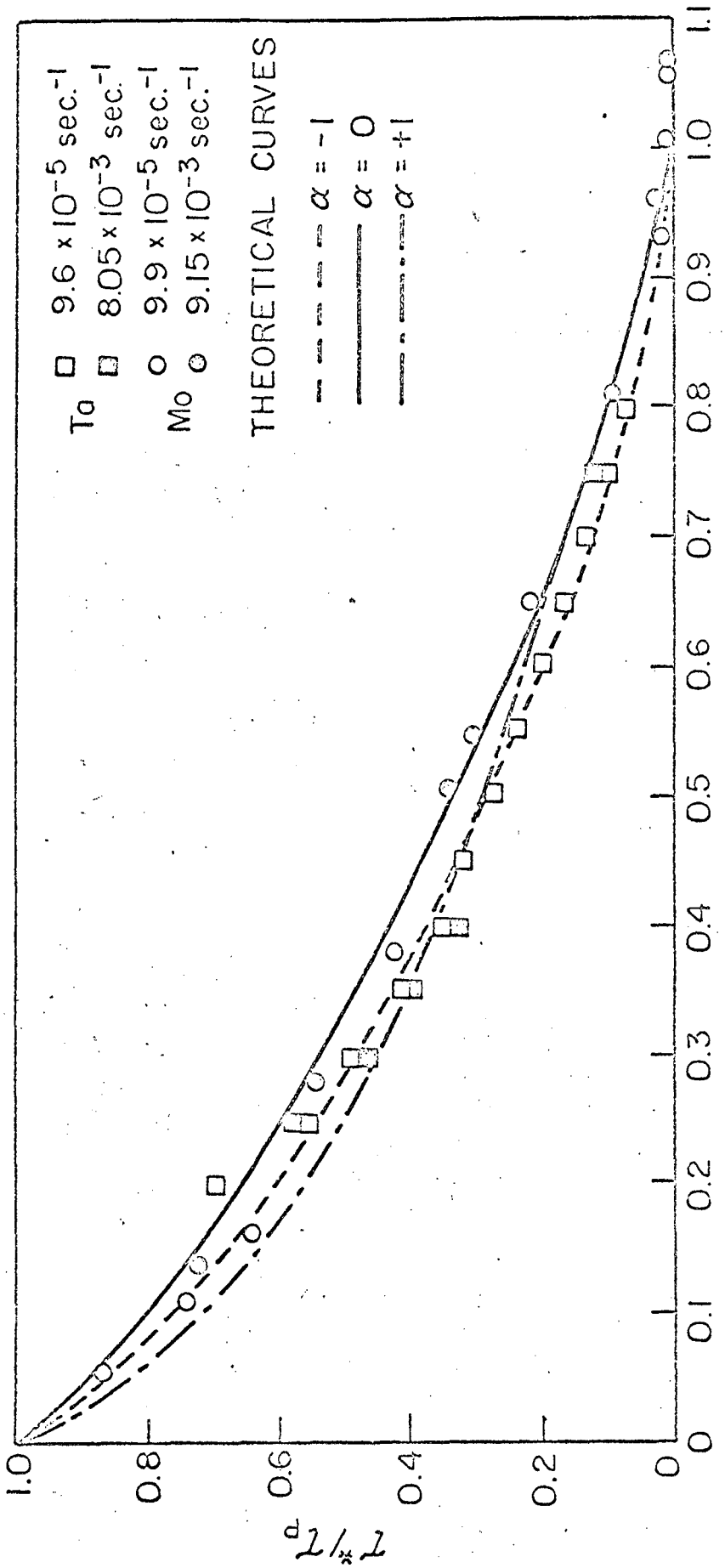
Ta □ 9.6 x 10⁻⁵ sec.⁻¹
□ 8.05 x 10⁻³ sec.⁻¹
Mo ○ 9.9 x 10⁻⁵ sec.⁻¹
○ 9.15 x 10⁻³ sec.⁻¹
THEORETICAL CURVES
α = -1
α = 0
α = +1
T/Tc
τ*/τp
0
0.1
0.2
0.3
0.4
0.5
0.6
0.7
0.8
0.9
1.0
1.1
0.2
0.4
0.6
0.8
1.0

Fig. 8

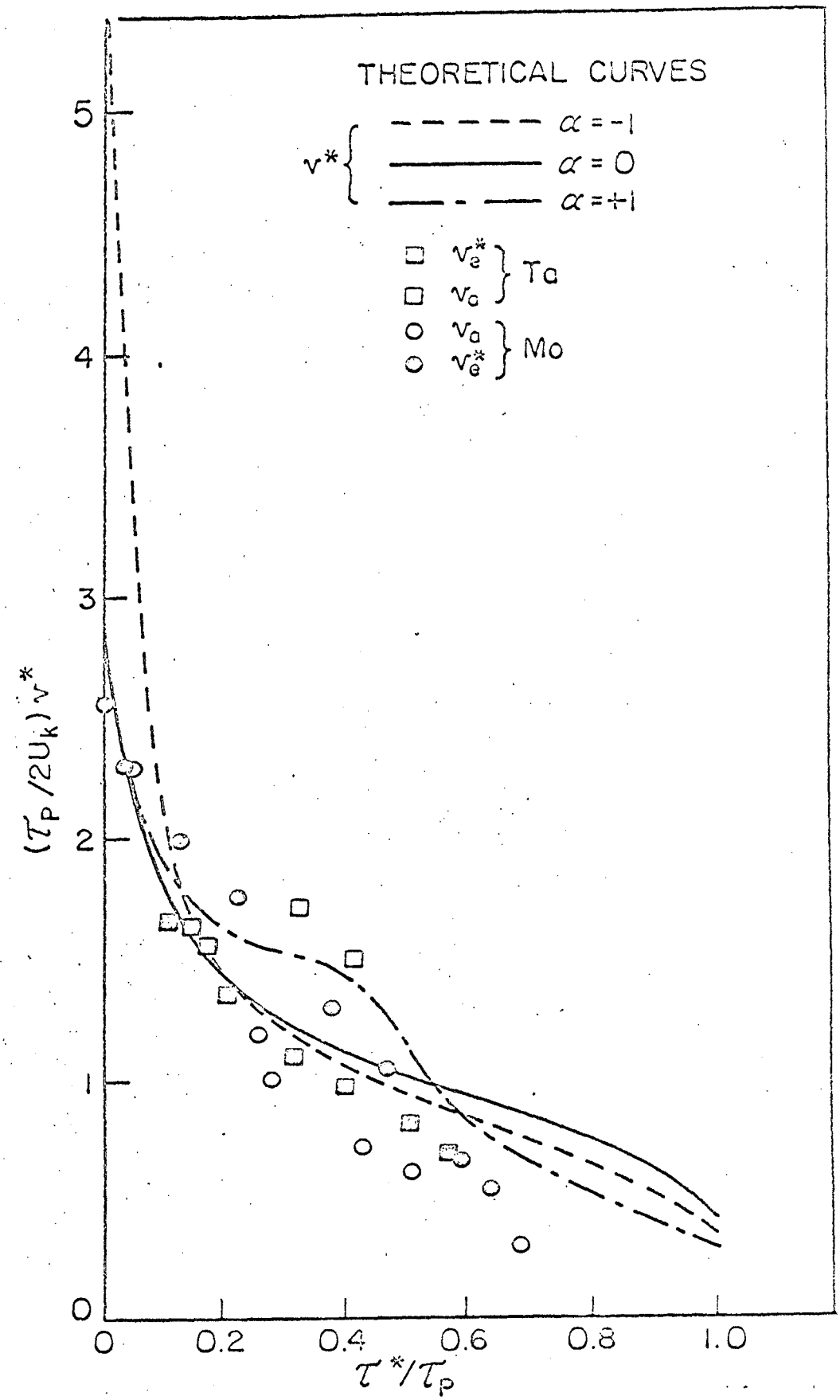
THEORETICAL CURVES
ν*
α = -1
α = 0
α = +1
ν*e
νa
Ta
νa
ν*e
Mo
(τp /2Uk) ν*
τ*/τp
0
0.2
0.4
0.6
0.8
1.0
1
2
3
4
5

Fig. 9

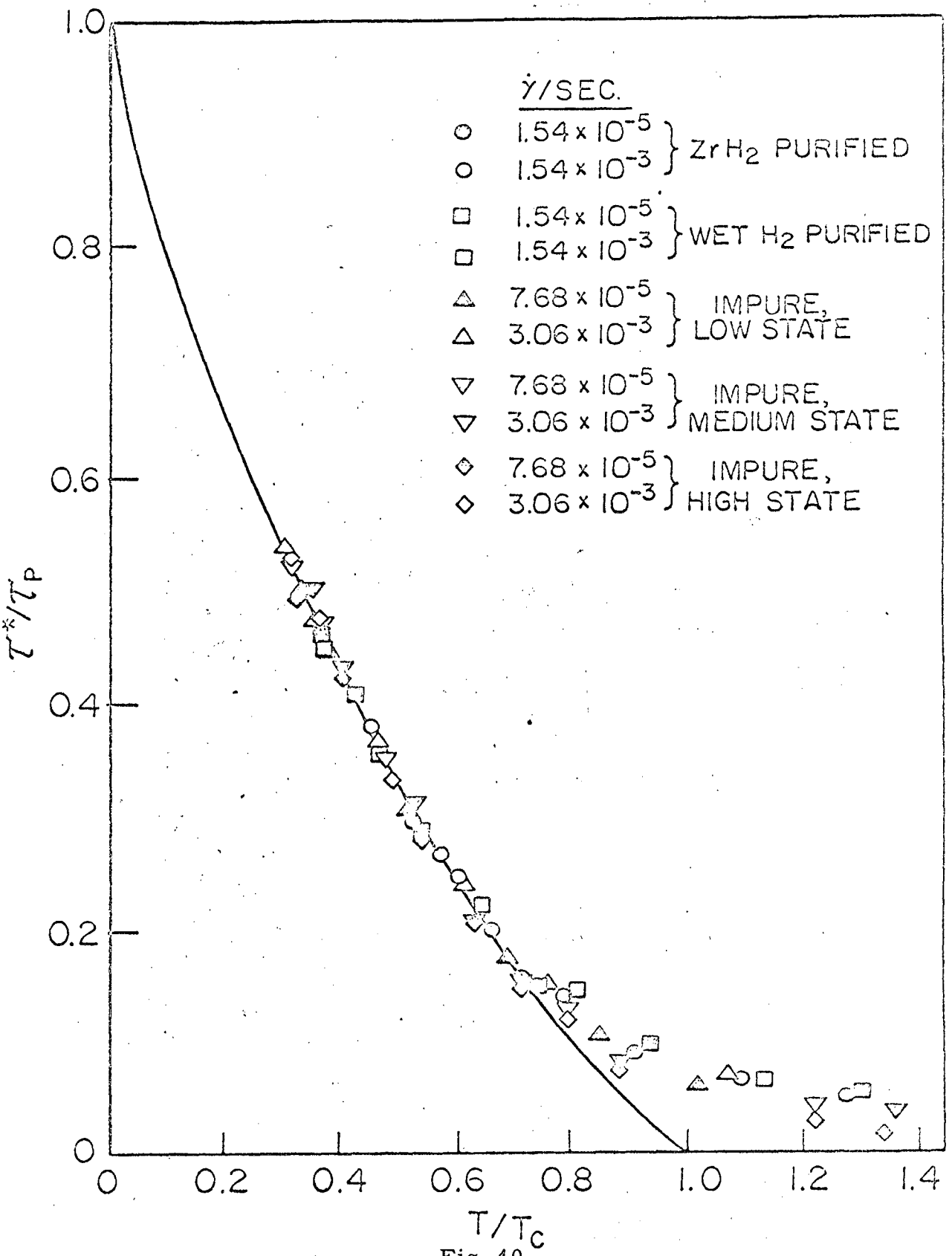
1.0
0.8
0.6
0.4
0.2
0
0
0.2
0.4
0.6
0.8
1.0
1.2
1.4
τ^*/τ_P
T/T_C
$\dot{\gamma}$/SEC.
1.54 x 10^{-5}
1.54 x 10^{-3}
ZrH$_2$ PURIFIED
1.54 x 10^{-5}
1.54 x 10^{-3}
WET H$_2$ PURIFIED
7.68 x 10^{-5}
3.06 x 10^{-3}
IMPURE, LOW STATE
7.68 x 10^{-5}
3.06 x 10^{-3}
IMPURE, MEDIUM STATE
7.68 x 10^{-5}
3.06 x 10^{-3}
IMPURE, HIGH STATE

Fig. 10

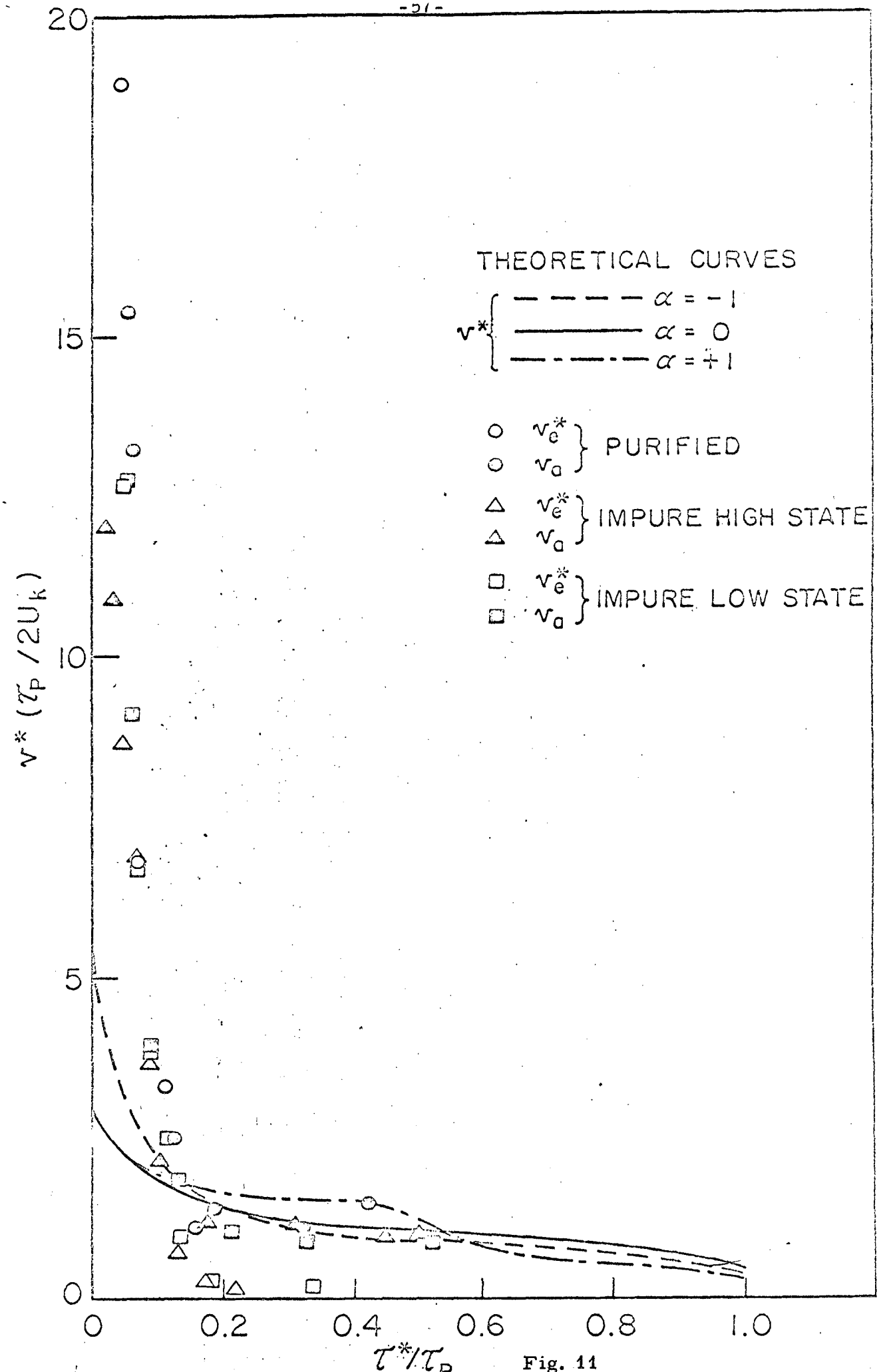
20
15
10
5
0
0
0.2
0.4
0.6
0.8
1.0
$\nu^*(\tau_p/2U_k)$
τ^*/τ_D
THEORETICAL CURVES
ν^* $\alpha = -1$
$\alpha = 0$
$\alpha = +1$
ν_e^* ν_a PURIFIED
ν_e^* ν_a IMPURE HIGH STATE
ν_e^* ν_a IMPURE LOW STATE

Fig. 11

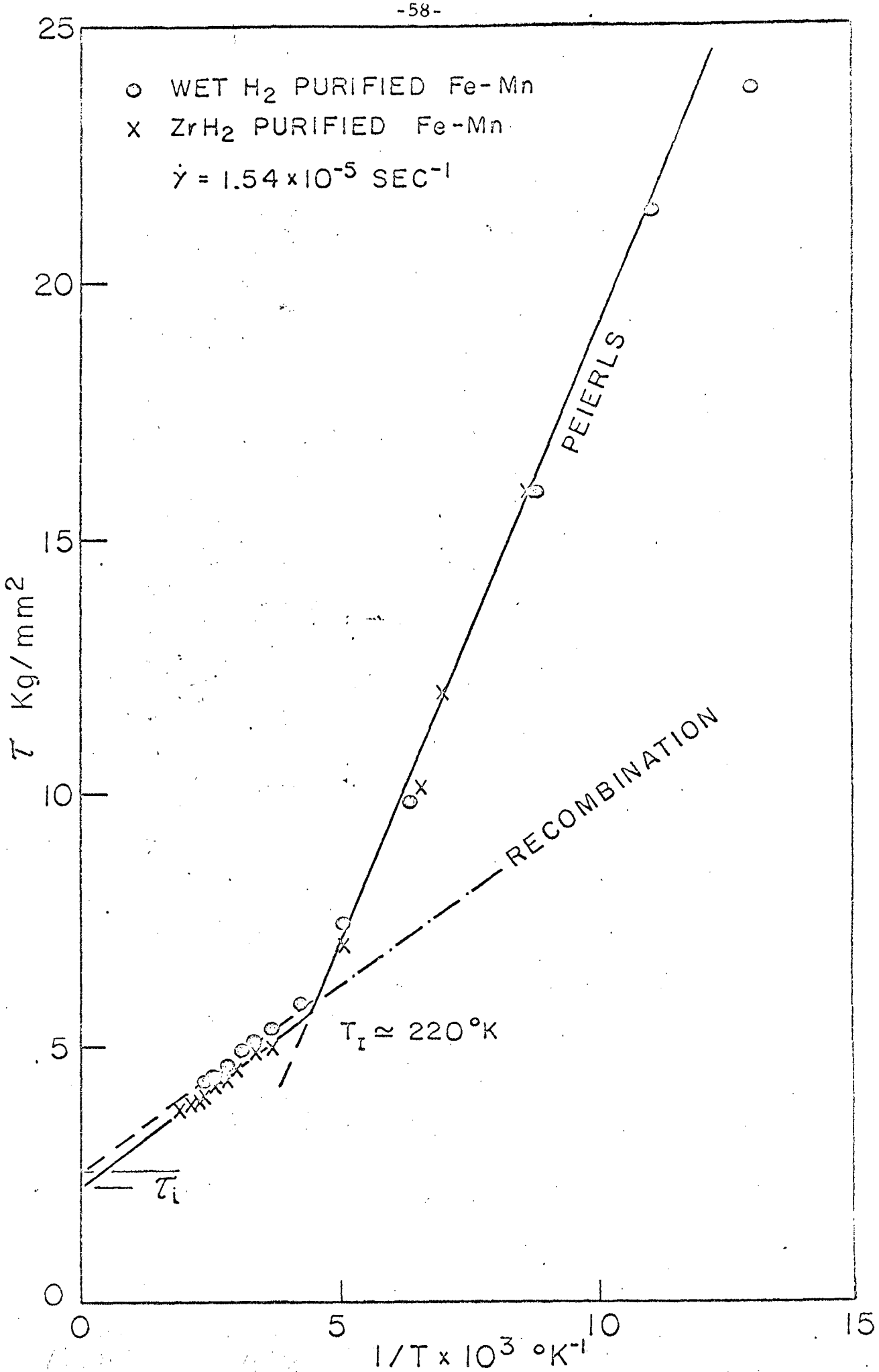
o WET H_2 PURIFIED Fe-Mn
x ZrH_2 PURIFIED Fe-Mn
$\dot{\gamma} = 1.54 \times 10^{-5}$ SEC^{-1}
PEIERLS
RECOMBINATION
$T_I \simeq 220$ °K
τ_i
τ Kg/mm^2
$1/T \times 10^3$ °K^{-1}
0
5
10
15
20
25

Fig. 12

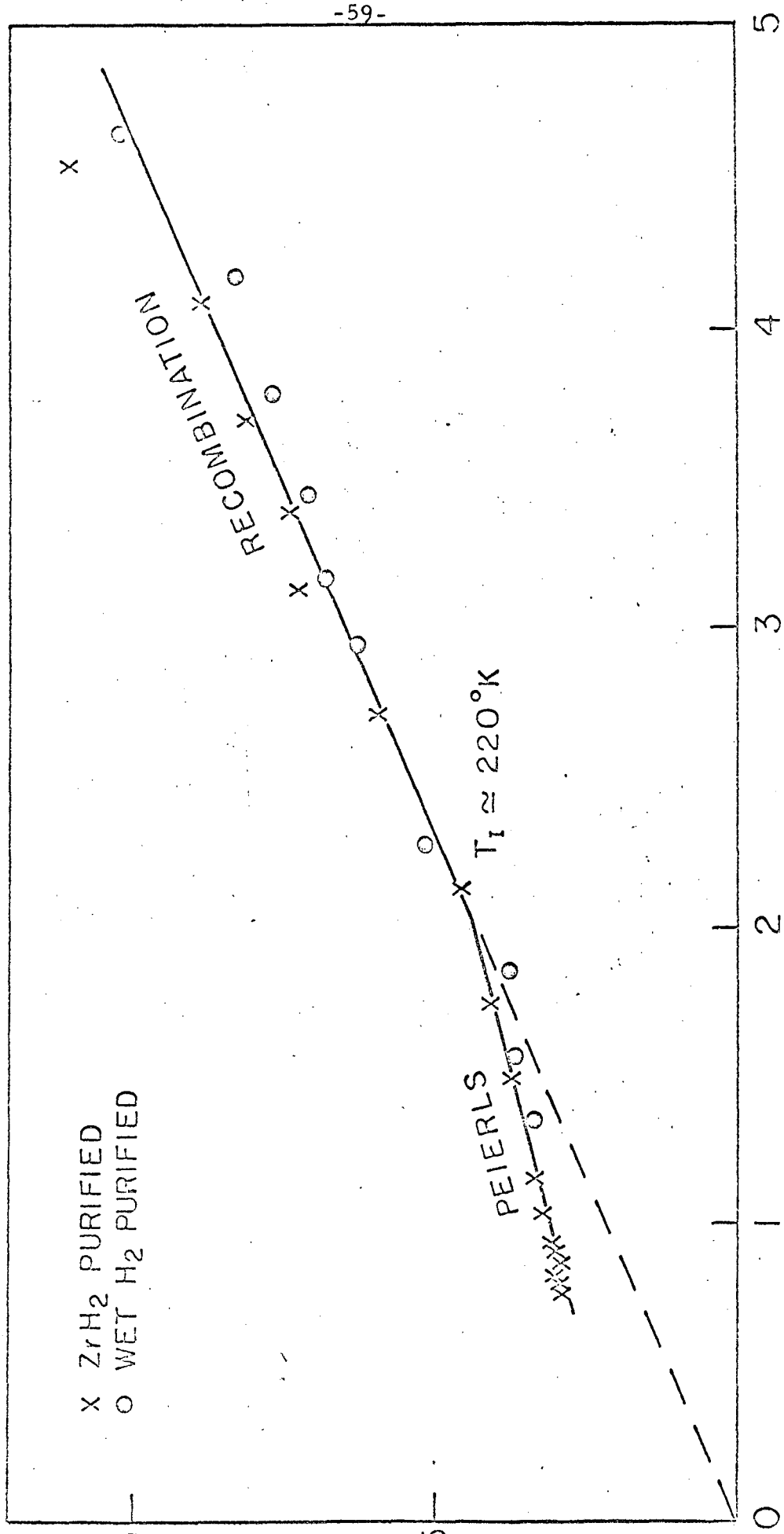
X ZrH2 PURIFIED
O WET H2 PURIFIED
RECOMBINATION
PEIERLS
T1 ≃ 220°K
1.0
0.5
0
0
1
2
3
4
5
1/τ* x 10^9 sec m^2/kg

Fig. 13

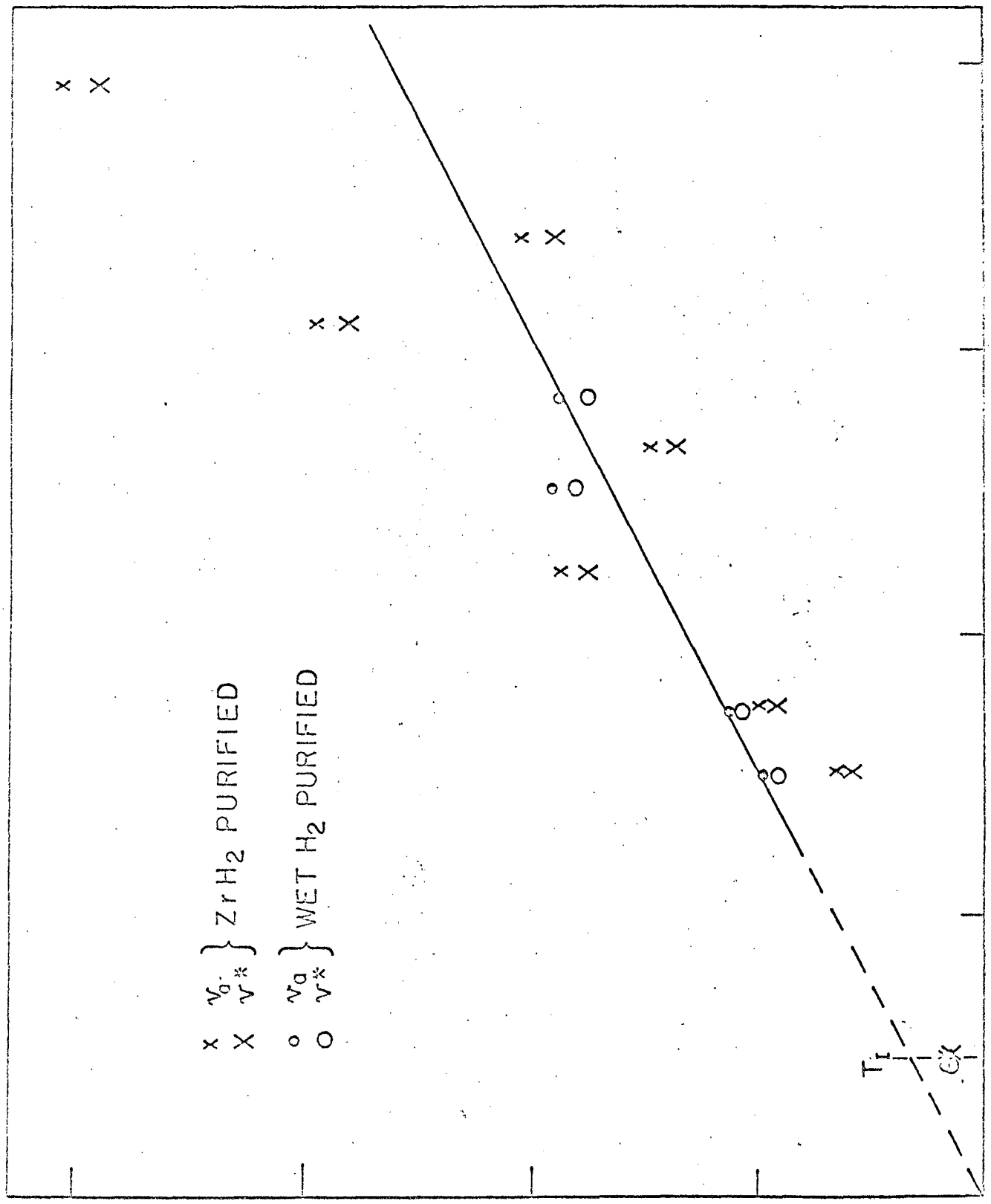
800
600
400
200
0
v^*/b^3
0
0.5
1.0
1.5
2.0
$1/\tau^{*2} \times 10^{17}$ m^4/kg^2
T_f
$\epsilon\chi$
ν_o
ν^*
Zr H_2 PURIFIED
ν_a
ν^*
WET H_2 PURIFIED

Fig. 14

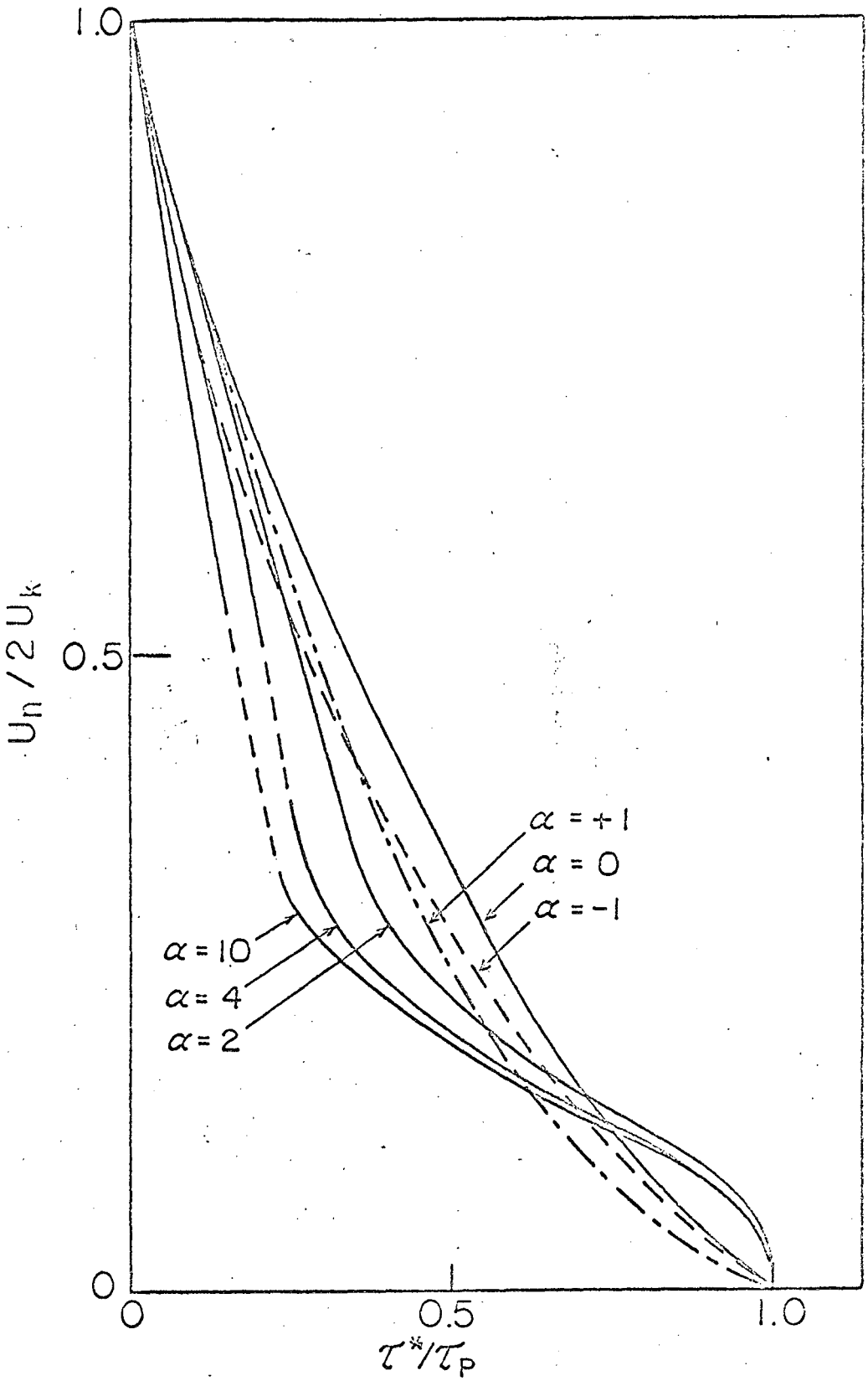
1.0
0.5
0
0
0.5
1.0
$U_n / 2U_k$
τ^*/τ_p
$\alpha = +1$
$\alpha = 0$
$\alpha = -1$
$\alpha = 10$
$\alpha = 4$
$\alpha = 2$

Fig. A2.1

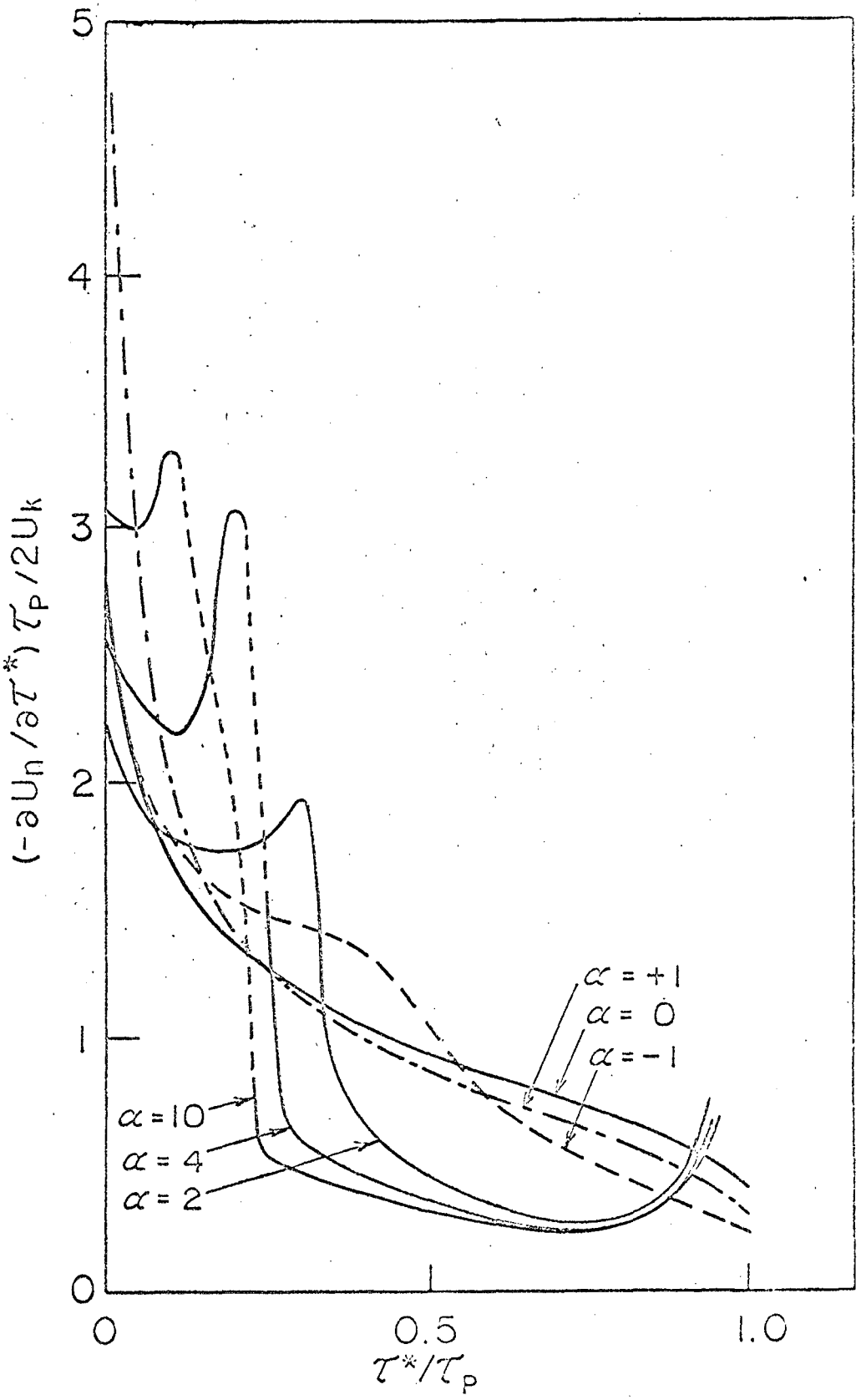
5
4
3
2
1
0
0
0.5
1.0
$(-\partial U_n/\partial \tau^*)\tau_p/2U_k$
τ^*/τ_p
$\alpha = +1$
$\alpha = 0$
$\alpha = -1$
$\alpha = 10$
$\alpha = 4$
$\alpha = 2$

Fig. A 2. 2